

We are IntechOpen, the world's leading publisher of Open Access books Built by scientists, for scientists

6,900

Open access books available

186,000

International authors and editors

200M

Downloads

Our authors are among the

154

Countries delivered to

TOP 1%

most cited scientists

12.2%

Contributors from top 500 universities



WEB OF SCIENCE™

Selection of our books indexed in the Book Citation Index
in Web of Science™ Core Collection (BKCI)

Interested in publishing with us?
Contact book.department@intechopen.com

Numbers displayed above are based on latest data collected.
For more information visit www.intechopen.com



Biomimetic Modifications of Calcium Orthophosphates

Diana Rabadjieva¹, Stefka Tepavitcharova¹,
Kostadinka Sezanova¹, Romyana Gergulova¹,
Rositsa Titorenkova², Ognyan Petrov² and Elena Dyulgerova³

¹*Institute of General and Inorganic Chemistry, Bulgarian Academy of Sciences, Sofia,*

²*Institute of Mineralogy and Crystallography, Bulgarian Academy of Sciences, Sofia,*

³*Faculty of Dental Medicine, University of Medicine, Sofia,
Bulgaria*

1. Introduction

Calcium orthophosphates are subject to intensive investigations owing to their biological importance. The ion-substituted non-stoichiometric nano-sized poorly crystalline calcium orthophosphates, mainly with apatite structure, build the inorganic component of hard tissues in the organisms. The main ion substitutes are the ions Na^+ , K^+ , Mg^{2+} , Fe^{2+} , Zn^{2+} , Si^{2+} , CO_3^{2-} , Cl^- , and F^- (Dorozhkin, 2009; Daculsi et al., 1997) and they differ in variety and amount depending on the type of the hard tissue, its age as well as on individual peculiarities. The so called “biological apatite” is formed in the living organisms as a result of biomineralization processes, the mechanism of which is not yet clarified. These processes include precipitation, dissolution and growth of poorly-crystalline calcium orthophosphates taking place in the organic matrix, e.g., collagen in the case of bones (Dorozhkin, 2009; Palmer et al., 2008) or amelogenin in the case of enamel (Palmer et al., 2008), in the presence of body fluids. One of the ways to elucidate the elementary processes occurring during bone hard tissue mineralization is the biomimetic approach designed to study these processes. The knowledge of the elementary processes is crucial for the development of new bioactive calcium phosphate materials (close to the natural ones) that may be applied for bone repairing, reconstruction and remodeling.

The aim of this chapter is to throw light on the biomimetic precipitation and modification of calcium orthophosphates, XRD-amorphous calcium phosphate (ACP) and dicalcium phosphate dihydrate (DCPD) on the basis of authors' kinetic, spectral (XRD and IR) and thermodynamic studies and literature data.

2. Calcium orthophosphates – short review

2.1 Classification

Eleven calcium orthophosphates are known in the literature. According to the methods of their preparation they are divided into two groups - calcium phosphates precipitates and calcium phosphates calcinates (Table 1). The preparation of calcium phosphates precipitates

strongly depends on pH of the medium; that of calcium phosphates calcinates is a function of the calcination temperature.

Abbreviation	Chemical formula	Ca/P	Preparation conditions
PRECIPITATES			pH
MCPM	$\text{Ca}(\text{H}_2\text{PO}_4)_2 \cdot \text{H}_2\text{O}$	0.5	0 - 2
MCPA	$\text{Ca}(\text{H}_2\text{PO}_4)_2$	0.5	
DCPD	$\text{Ca}(\text{HPO}_4)_2 \cdot 2\text{H}_2\text{O}$	1.0	2 - 6
DCPA	$\text{Ca}(\text{HPO}_4)_2$	1.0	
OCP	$\text{Ca}_8(\text{PO}_4)_4(\text{HPO}_4)_2 \cdot 5\text{H}_2\text{O}$	1.33	5.5 - 7
ACP	$\text{Ca}_9(\text{PO}_4)_6 \cdot n\text{H}_2\text{O}$	1.5	5 - 12
PCA	$\text{Ca}_{10-x} \square_x (\text{PO}_4)_{6-x} (\text{HPO}_4)_x \cdot ((\text{OH})_{2-x} \square_x)$	1.33-1.67	6.5 - 9.5
HA	$\text{Ca}_{10}(\text{PO}_4)_6(\text{OH})_2$	1.67	9.5 - 12
CALCINATES			T, °C
TCP	$\beta\text{-Ca}_3(\text{PO}_4)_2$	1.5	>800
	$\alpha\text{-Ca}_3(\text{PO}_4)_2$	1.5	>1125
TTCP	$\text{Ca}_4(\text{PO}_4)_2\text{O}$	2.0	>1500

^a the table was adapted according to Dorozhkin (2009), Chow and Eanes (2001) and Johnsson and Nancollas (1992).

Table 1. Calcium orthophosphates^a.

2.2 Structures

Calcium phosphates are divided into three groups according to their structure (Chow & Eanes, 2001): (i) Ca-PO₄ sheet-containing compounds (MCPA, MCPM, DCPA DCPD). DCPD has a monoclinic structure, space group *Ia*, where HPO₄²⁻ ions are linked to Ca²⁺ ions forming linear chains, that are stacked and form corrugated sheets parallel to the (010) face. The water molecules are situated between the sheets, bonded to the Ca²⁺ ion. The packing of the Ca-HPO₄ ions in chains or sheets determine several possible pseudo-hexagonal arrangements, similar to the glaserite type structure (Curry & Jones, 1971; Dickens et al., 1972; Dickens & Bowen, 1971); (ii) glaserite type compounds (α -TCP and β -TCP). Two types of columns along the c-axis in a pseudo-hexagonal arrangement, one containing only Ca²⁺ and other both Ca²⁺ and PO₄³⁻ ions in a ratio 1:2 build the glaserite type structure of monoclinic α -TCP (Mathew et al., 1977). In rhombohedral β -TCP structure two types of columns contain both Ca²⁺ and PO₄³⁻ ions (Dickens et al., 1974). One of the columns has vacancies at both cationic and anionic position; and (iii) apatite type compounds (OCP, TTCP, PCA and HA) (Chow & Eanes 2001; Mathai&Takagi, 2001). Commonly, HA has a hexagonal structure (space group *P63/m*) (Kay et al., 1964), where Ca²⁺ ions occupy two different crystallographic symmetry sites. Ca1 are located in columns along the c-axis, where is coordinated to nine O atoms. The Ca-O₉ polyhedra are connected in chains parallel to c-axis. Ca2 are arranged in two triangular units. The Ca2 ions are 7-coordinated, with six O atoms and one OH⁻ ion. Ca1 and Ca2 polyhedra are linked through oxygen atoms of the PO₄³⁻ tetrahedra. Each OH⁻ ion occupies statistically disordered positions.

OCP has a triclinic structure, which can be described as alternating along (100) “hydrated” and apatitic layers (Mathew et al., 1988). The atomic positions of the structure of OCP are very close to HA structure, which is the precondition for possible epitaxial growth and formation of interlayered structures, important for explanation of the process of biomineralization.

A special position holds the amorphous calcium phosphate (ACP) which structure is built of $\text{Ca}_9(\text{PO}_4)_6$, so called Posner’s clusters, where Ca^{2+} and PO_4^{3-} ions are arranged in a hexagonal dense packing (Betts et al., 1975; Blumenthal et al., 1977).

The existing symmetry relations between these structures ensure the easier phase transformations.

2.3 Solubility

Calcium orthophosphates are sparingly soluble in water (Table 2). HA has the lowest solubility among them, which is its natural priority. The solubility of calcium phosphates strongly depends on pH of the medium and this feature is of significance for their preparation and biological behavior. Thus, the practically insoluble mono-phase bio-ceramics of dense HA do not actively participate in the process of bone remodeling (Tas, 2004). However, upon contact with body fluids they participate in the formation of a surface layer of bone-like apatite. Mono-phase α -TCP and β -TCP display higher solubilities and rapidly degrade *in vitro* and *in vivo* (Radin & Ducheyne, 1993, 1994). Mg- and Zn-doped TCP ceramics display lower solubility than pure TCP ceramics and thus reduce the resorption rate (Xue, 2008). Bi-phase mixtures of HA and β -TCP ceramics were developed in order to improve the biological behaviour of the mono-phase materials (Petrov et al., 2001; Teixeira et al., 2006).

The knowledge on the Ca^{2+} , H^+ / OH^- , PO_4^{3-} // H_2O system and its sub-systems may be used as a theoretical base for predetermination or optimization of the conditions for the preparation of different calcium orthophosphates. Unfortunately, owing to the low solubility and narrow crystallization fields of the different stable and metastable salts, there are no systematic experimental studies of this system. Only single solubility data are available for the binary sub-system Ca^{2+} / PO_4^{3-} // H_2O at 25°C (Kirgintzev et al., 1972). More detailed studies were performed on the three-component Ca^{2+} , H^+ / PO_4^{3-} // H_2O sub-system and experimental data are available for the temperature range 0 – 100°C (Flatt et al., 1961; Bassett, 1958; Flatt et al., 1956; Chepelevskii et al., 1955; Belopol’skii, 1940; Bassett, 1917). Two hydrous and two anhydrous salts, namely $\text{Ca}(\text{H}_2\text{PO}_4)_2$, $\text{Ca}(\text{H}_2\text{PO}_4)_2 \cdot \text{H}_2\text{O}$, CaHPO_4 and $\text{CaHPO}_4 \cdot 2\text{H}_2\text{O}$ are established at 25°C and 40°C respectively; there are contradictions about the existence and stability of the salt of lowest solubility $\text{CaHPO}_4 \cdot 2\text{H}_2\text{O}$ (Bassett, 1917; Belopolskii et al., 1940; Chepelevskii et al., 1955). The solubility of $\text{Ca}(\text{H}_2\text{PO}_4)_2$ and $\text{Ca}(\text{H}_2\text{PO}_4)_2 \cdot \text{H}_2\text{O}$ slightly increases at temperatures above 50°C but $\text{CaHPO}_4 \cdot 2\text{H}_2\text{O}$ was not detected (Bassett, 1917; Chepelevskii et al., 1955).

The most appropriate method for evaluation of the solubility of sparingly soluble calcium phosphate salts is the thermodynamic modeling. The ion association model based on the extended Debye-Huckel theory was applied to the Ca^{2+} , H^+ / OH^- , PO_4^{3-} // H_2O system (Chow & Eanes, 2001; Johnson & Nancollas, 1992). Thermodynamic data for the solubility products ($\lg K_{\text{sp}}^0$) of all calcium orthophosphates and the complex formation constants ($\lg K^0$) of all complex species which may exist in aqueous calcium phosphate solutions are necessary for its application (Table 2). The calculations of Chow and Eanes (2001) have

shown that DCPA is the least soluble salt in the Ca^{2+} , H^+/OH^- , $\text{PO}_4^{3-}/\text{H}_2\text{O}$ system at $\text{pH} < 4.2$ and 25°C while HA becomes the least soluble salt at $\text{pH} > 4.2$; TTCP is the most soluble salt at $\text{pH} < 8.2$ while DCPD is the most soluble salt at $\text{pH} > 8.2$. In the pH region 7.3 - 7.4 typical for body fluids, the solubility of the salts at 25°C (Chow & Eanes, 2001) and 37°C (Johnson & Nancollas, 1992) follows the order:



Chemical formula	Solubility, g/l, 25°C (Dorozhkin, 2009)	$-\lg K_{\text{sp}}^0$
$\text{Ca}(\text{H}_2\text{PO}_4)_2 \cdot \text{H}_2\text{O}$	~18	1.14 (Fernandez et al., 1999)
$\text{Ca}(\text{H}_2\text{PO}_4)_2$	~17	1.14 (Fernandez et al., 1999)
$\text{CaHPO}_4 \cdot 2\text{H}_2\text{O}$	~0.088	6.59 (Gregory et al., 1970)
CaHPO_4	~0.048	6.90 (McDowell et al., 1971)
$\text{Ca}_8\text{H}_2(\text{PO}_4)_6 \cdot 5\text{H}_2\text{O}$	~0.0081	96.6 (Tung et al., 1988)
$\text{Ca}_3(\text{PO}_4)_2(\text{am})$	-	25.2 (Meyer & Eanes 1978)
$\text{Ca}_5(\text{PO}_4)_3\text{OH}$	~0.0003	58.4 (McDowell et al., 1977)
$\alpha\text{-Ca}_3(\text{PO}_4)_2$	~0.0025	25.5 (Fowler & Kuroda, 1986)
$\beta\text{-Ca}_3(\text{PO}_4)_2$	~0.0025	28.9 (Gregory et al., 1974)
$\text{Ca}_4(\text{PO}_4)_2\text{O}$	~0.0007	38.0 (Matsuya et al., 1996)
<i>Complex formation constants</i> (National Institute of Standards and Technology [NIST], 2003)		
$\text{H}^+ + \text{H}_2\text{PO}_4^- = \text{H}_3\text{PO}_4^0$		2.148
$\text{H}^+ + \text{HPO}_4^{2-} = \text{H}_2\text{PO}_4^-$		7.198
$\text{H}^+ + \text{PO}_4^{3-} = \text{HPO}_4^{2-}$		12.37
$\text{Ca}^{2+} + \text{OH}^- = \text{CaOH}^+$		1.303
$\text{Ca}^{2+} + \text{HPO}_4^{2-} = \text{CaHPO}_4^0$		2.66
$\text{Ca}^{2+} + \text{H}_2\text{PO}_4^- = \text{CaH}_2\text{PO}_4^+$		1.35
$\text{Ca}^{2+} + \text{PO}_4^{3-} = \text{CaPO}_4^-$		6.46

Table 2. Solubility and thermodynamic data of the Ca^{2+} , H^+/OH^- , $\text{PO}_4^{3-}/\text{H}_2\text{O}$ system.

3. Electrolyte systems for biomimetic studies

Electrolyte solutions of different composition, designed to mimic the acellular human body plasma, have become a modern way to test bone-bonding abilities of bioactive materials or to produce thin calcium-phosphate layers on materials (metals, alloys or glasses) for bone graft substitutes (Yang & Ong, 2005; Raghuvir et al., 2006; Jalota et al., 2006; Kontonasaki et al., 2002). The composition of the most popular ones is presented in Table 3.

Earle's balanced salt solution (EBSS, $\text{Ca}/\text{P} = 1.8$, $\text{HCO}_3^- - 26.2 \text{mmol} \cdot \text{dm}^{-3}$) (Earle et al., 1943) and Hank's balanced salt solution (HBSS, $\text{Ca}/\text{P} = 1.6$, $\text{HCO}_3^- - 4.2 \text{mmol} \cdot \text{dm}^{-3}$) (Hanks & Wallace, 1949) were among the first simulated body solutions. Kokubo (1990) was the first to popularize a multicomponent inorganic solution, called conventional simulated body fluid (SBF) which contains definite amounts of Na^+ , K^+ , Mg^{2+} , Ca^{2+} , Cl^- , HCO_3^{2-} , HPO_4^{2-} and SO_4^{2-} ions, has a Ca/P ratio of 2.5 (equal to that in the blood plasma), HCO_3^- concentration of $4.2 \text{mmol} \cdot \text{dm}^{-3}$ and physiologic pH of 7.3-7.4. To mimic the blood plasma in terms of the most important HCO_3^- ions, Bayractor and Tas (1999) revised the SBF by increasing HCO_3^-

concentration up to 27 mmol.dm⁻³ at the account of Cl⁻ ions (revised simulated body fluid, SBFr). The concentrations of Ca²⁺ and Mg²⁺ ions in the ionic SBF (SBFi) correspond to those of free Ca²⁺ and Mg²⁺ ions (not bound to proteins), in the blood plasma (Oyane, et al., 2003).

Ion content	Blood Plasma	EBSS (Earle, et al., 1943)	HBSS (Hanks and Wallace, 1949)	SBFc (Kokubo, 1990)	SBFr (Bayraktar and Tas, 1999)	SBFi (Oyane, et al., 2003)	SBFg (this study)
Na ⁺	142.0	143.5	142.1	142.0	142.0	142.0	142.0
K ⁺	5.0	5.4	5.3	5.0	5.0	5.0	5.0
Ca ²⁺	2.5	1.8	1.26	2.5	2.5	1.6	2.5
Mg ²⁺	1.5	0.8	0.9	1.5	1.5	1.0	1.5
Cl ⁻	103.0	123.5	146.8	147.8	125.0	103.0	147.8
HCO ₃ ²⁻	27.0	26.2	4.2	4.2	27.0	27.0	4.2
HPO ₄ ²⁻	1.0	1.0	0.78	1.0	1.0	1.0	1.0
Glycine	-	-	-	-	-	-	135.0
SO ₄ ²⁻	0.5	0.8	0.41	0.5	0.5	1.5	0.5
Ca/P	2.5	1.8	1.62	2.5	2.5	1.6	2.5
pH	7.4	7.2-7.6	6.7-6.9	7.2-7.4	7.4	7.4	7.3

Table 3. Electrolyte solutions for in vitro experiments, mmol.dm⁻³.

These solutions were buffered to the pH of blood plasma with TRIS, BITRIS or HEPES buffers.

SBF modified with glycine (SBFg), essential for the biological system amino acid, was prepared on the basis of conventional SBF. Concentration of glycine was thermodynamically calculated so that the contents of free Ca²⁺ and Mg²⁺ ions to be analogous to SBFi.

4. Biomimetic precipitation of ion modified precursors

The biomimetic approach which includes precipitation processes of bioactive calcium phosphates in electrolyte medium of simulated body fluids and uses the influence of the medium composition on their formation and phase transformation have attracted extensive research interest (Xiaobo et al., 2009; Hui et al., 2009; Shibli & Jayalekshmi, 2009; Martin et al., 2009), because of their analogy to the biological mineralization processes. In the following, the authors' studies on the precipitation of ion-modified ACP and DCPD precursors are summarized.

Various crystal chemical and kinetic factors affect the crystallization process. The ion-modified calcium phosphates are mixed crystals (non-stoichiometric compounds), where part of the ions building the crystal unit cell are substituted by other ions. The ability of the admixture ion to adopt the coordination of the substituted ion determines the substitution degree.

To enable ion modification of calcium phosphate precursors with Na⁺, K⁺, Mg²⁺ and Cl⁻ ions we have performed all our studies using conventional SBFc that was modified for each concrete case. Modified calcium-free simulated body fluid (SBFc-Cam) was used as a solvent for K₂HPO₄ (Solution 1) and phosphorus-free simulated body fluid (SBFc-Pm) was used as a solvent for CaCl₂ (Solutions 2 and 5), for CaCl₂ and MgCl₂ (Solution 3) and for ZnCl₂

(Solution 4) (Table 4). In this way preliminary precipitation was avoided. pH of the mixed solutions was adjusted to 7.2-7.4 using 0.1M HCl or 0.05M 2-amino-2-hydroxymethyl-1,3-propandiol.

Ion content	<i>SBFc-Cam</i> (Solution 1)	<i>SBFc-Pm</i> *(Solution 2)	<i>SBFc-Pm</i> (Solution 3)	<i>SBFc-Pm</i> (Solution 4)	<i>SBFc-Pm</i> **(Solution 5)
Na ⁺	141.9	141.9	141.9	141.9	141.9
K ⁺	506.4	3.0	3.0	3.0	5.0
Mg ²⁺	1.5	1.5	1.5	1.5	1.5
Ca ²⁺	-	418.9 - x	418.9 - x		252.1
Me ²⁺	-		x	x	
Cl ⁻	142.8	975.6 - 2x	975.6	142.8 + 2x	642.0
SO ₄ ²⁻	0.5	0.5	0.5	0.5	0.5
HCO ₃ ⁻	4.2	4.2	4.2	4.2	4.2
HPO ₄ ²⁻	251.7	-	-	-	0.00

* - in the case of ACP precipitation; ** - in the case of DCPD precipitation;
 $0 < x < 83.8 \text{ mmol.dm}^{-3}$.

Table 4. Modified simulated body fluids (SBFs) (mmol.dm^{-3}) used by the authors.

The electrolyte medium provided by SBF plays a crucial role in the precipitation processes and influences the composition of the precipitated product. Precipitation, co-precipitation, ion substitution and ion incorporation reactions simultaneously take place. The cationic and anionic substitutions are mainly responsible for the calcium deficiency of the precipitated ACP precursors. Two methods – fast mixing or continuous co-precipitation of the reagents were applied in these studies. The method of precipitation affected the size, morphology and chemical homogeneity of the precipitate.

SBF-modified XRD-amorphous calcium-deficient phosphate (ACP) (Fig. 1) with a Ca/P ratio of 1.3 or 1.51 (Table 5) due to ion substitution and incorporation of Na⁺, K⁺, Mg²⁺ and Cl⁻ ions from the SBFs at levels close to those of natural enamel, dentin and bone (Dorozhkin, 2009), was precipitated.

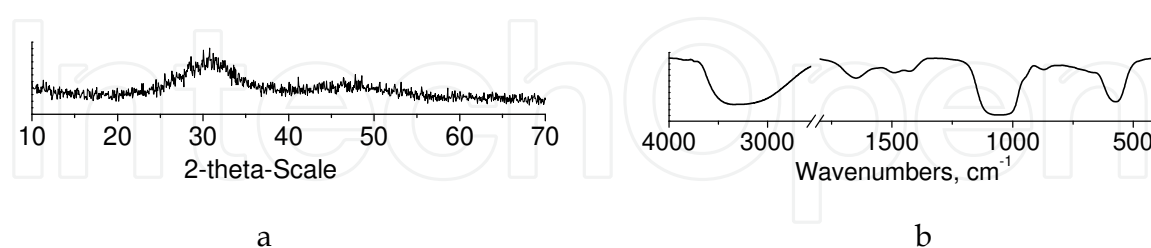


Fig. 1. XRD (a) and IR (b) spectra of SBF modified amorphous calcium phosphate.

The fast precipitation was carried out by mixing Solution 1 and Solution 2 (Table 4) at a Ca/P ratio of 1.67 and pH of 11.5 (maintained by 1M KOH) under intense stirring at room temperature. It is known that the fast mixing, the high supersaturation and the presence of Mg²⁺ and CO₃²⁻ ions provoke the precipitation of an amorphous calcium-deficient product (Sinyaev et al., 2001; Combes & Rey, 2010). The continuous co-precipitation was carried out by mixing Solution 1 and Solution 2 (Table 4) at a rate of 3 ml/min to precipitate in glycine buffer (Sykora, 1976) at room temperature and pH 8 (maintained by 1M KOH).

Mg mmol/g	Na mmol/g	K mmol/g	Cl mmol/g	Mg/Ca	Ca/P	(Ca+Mg+Na+K)/P
Biomimetic precipitated ACP at quick mixing						
0.13	0.20	0.45	0.03	0.03	1.51	1.79
Biomimetic precipitated ACP at continuous co-precipitation						
0.04	0.05	0.01	0.05	0.005	1.3	1.33
Enamel, Dentin, Cementum, Bone (Dorozhkin, 2009)						
0.02 - 0.29	0.22 - 0.39	2.10 ⁻⁴ - 0.02	0.03 - 0.1	0.03 - 0.06	1.61 - 1.77	

Table 5. Compositions of ACP precursor and natural Enamel, Dentin, Cementum and Bone.

Zn- or Mg-modified amorphous calcium phosphate precursors with varying $Me^{2+}/(Ca^{2+}+Me^{2+})$ ratio from 0.01 to 0.16 (Table 6) due to Ca^{2+} ion substitution by Me^{2+} ions as well as Me^{2+} incorporation were precipitated by the method of continuous co-precipitation in electrolyte system only. All reagents (Solutions 1, 2 and 4 for Zn-modified precursors and Solutions 1 and 3 for Mg-modified precursors, Table 4) with a $(Ca^{2+}+Me^{2+})/P$ ratio of 1.67 ($Me^{2+} = Mg, Zn$) were mixed to precipitate in glycine buffer with a rate of 3 ml/min at room temperature and pH 8 (maintained by 1M KOH). The modified conventional simulated body fluids provided ion modification of all Mg- and Zn-modified calcium phosphate precursors with Na^+ (0.02 - 0.08 mmol/g), K^+ (0.01 - 0.02 mmol/g), Mg^{2+} (0.04 mmol/g) and Cl^- (below 0.05 mmol/g) ions (Table 6).

Sample	Liquid phase	Solid phase						
	$Me^{2+}/(Me^{2+}+Ca^{2+})$ in initial solutions	$Me^{2+}/(Me^{2+}+Ca^{2+})$	$(Ca^{2+}+Mg^{2+}+Zn^{2+}+Na^++K^+)/P$	Zn^{2+} , mmol/g	Mg^{2+} , mmol/g	Na^+ , mmol/g	K^+ , mmol/g	Cl^- , mmol/g
Zinc-modified calcium phosphates								
Zn1	0.01	0.01	1.31	0.09	0.03	0.03	0.01	<0,05
Zn3	0.03	0.03	1.35	0.29	0.05	0.04	0.02	<0,05
Zn5	0.05	0.05	1.35	0.41	0.04	0.05	0.02	<0,05
Zn10	0.10	0.10	1.31	0.90	0.06	0.02	0.01	<0,05
Zn13	0.13	0.13	1.40	1.19	0.05	0.08	0.02	<0,05
Magnesium-modified calcium phosphates								
Mg2	0.03	0.02	1.36	-	0.21	0.05	0.02	<0,05
Mg5	0.10	0.05	1.35	-	0.45	0.08	0.01	<0,05
Mg10	0.13	0.10	1.33	-	0.85	0.06	0.02	<0,05
Mg16	0.20	0.16	1.38	-	1.45	0.04	0.02	<0,05

Table 6. Ion content of the magnesium- and zinc- modified calcium phosphates and their initial solutions.

By analogy with Bigi et al. (1995), we have established that the presence of Zn^{2+} or Mg^{2+} ions in the reaction mixture inhibits the crystallization of HA, so that XRD amorphous Mg- or Zn-modified calcium phosphate precursors are obtained. The Posner's clusters (Betts et al.,

1975; Blumenthal et al., 1977) of the complex formula $\text{Ca}_w\text{Mg}_x\text{Zn}_y\text{Na}_z\text{K}_u(\text{PO}_4)_v(\text{CO}_3)_{6-v}$ ($w+x+y+z+u \leq 9$) are the first particles formed in the studied complex electrolyte $\text{SBF} - \text{CaCl}_2 - \text{MgCl}_2/\text{ZnCl}_2 - \text{KOH} - \text{H}_2\text{O}$ system. A modifying ion, whose ionic radius and electrical charge are closer to those of the Ca^{2+} ions, will be more readily incorporated into the Pozner's clusters. The Zn^{2+} ionic radius (0.74 Å) is closer to that of the Ca^{2+} ion (1.0 Å) than the radius of the Mg^{2+} ion (0.65 Å). The substitution with Na^+ (0.95 Å) and K^+ (1.33 Å) ions is partial not only for geometrical reasons but also for electrostability. The results (Table 6) showed that all Zn^{2+} ions and only about half of the Mg^{2+} ions from the reaction solutions were included in the precipitated ACP. The different chemical behavior of Zn^{2+} and Mg^{2+} ions can be explained by the "softness-hardness" factor and by the Crystal Field Stabilization Energy (CFSE). According to Pearson's concept of "hard" and "soft" Lewis acids and bases (Pearson, 1963), as well as the Klopman scale of hardness and softness (Klopman, 1968), "soft acids" predominantly coordinate "soft bases" and "hard acids" - predominantly "hard bases". Mg is a "hard acid", while Zn is a "soft acid". The simulated body fluids contain high concentrations of Cl^- ions which are "softer bases" than H_2O , OH^- , PO_4^{3-} , SO_4^{2-} , HCO_3^- and HPO_4^{2-} . Although Zn^{2+} ions are a "soft acid", they form a negligible amount of chloride complexes due to the zero value of their CFSE and mainly exist as free Zn^{2+} ions in the studied solutions. In contrary, Mg^{2+} as a "hard acid" is preferentially coordinated by the H_2O molecules ("hard base") and are mainly present as $[\text{Mg}(\text{H}_2\text{O})_6]^{2+}$ complexes. The last ones are too large to be incorporated into the crystal structure of the calcium phosphate without its distortion. The necessity of overcoming the energy barrier for even partial dehydration of the $[\text{Mg}(\text{H}_2\text{O})_6]^{2+}$ complexes is another reason for the low substitution rate of these ions.

DCPD biomimetic precipitated precursors - Well crystallized dicalcium phosphate dihydrate (DCPD) (Fig.2) was precipitated by the method of fast mixing (room temperature and intense stirring) of Solution 1 and Solution 5 (Table 4) at a Ca/P ratio of 1 and pH 6 (maintained by 1M HCl). Differently from all modified ACP precursors, only negligible amounts of Mg^{2+} (0.001 mmol/g), Na^+ (0.025 mmol/g), K^+ (0.001 mmol/g) and Cl^- (0.003 mmol/g) ions were found in biomimetic precipitated DCPD.

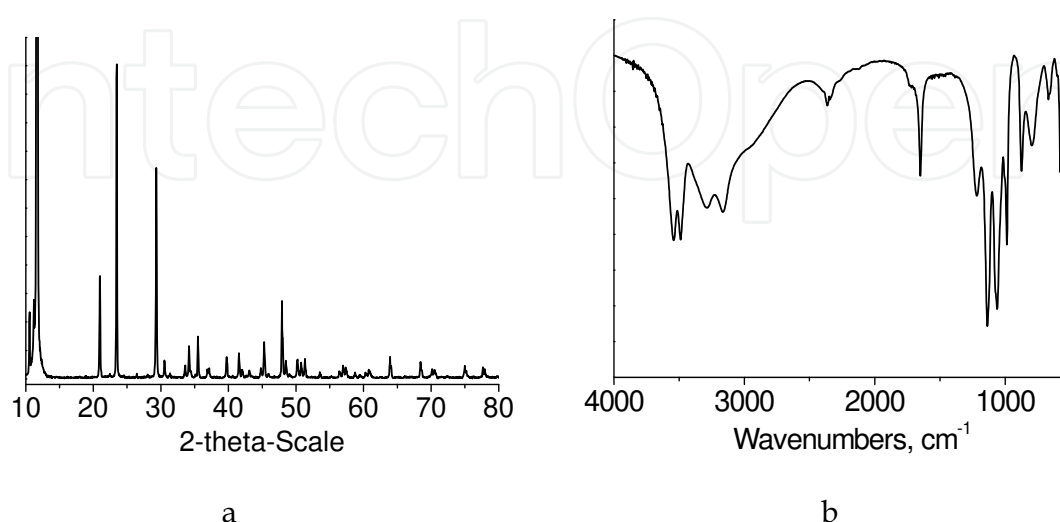


Fig. 2. XRD (a) and IR (b) spectra of precipitated DCPD.

Thermodynamic modeling of biomimetic precipitation - The precipitation processes of SBF-modified ACP and DCPD as well as of Zn- and Mg-modified ACP were simulated by an ion-association model using the computer program PHREEQCI v.2.14.3 (Parkhurst, 1995). All possible association/dissociation and dissolution/ crystallization processes in the SBFs were taken into account. The formation of complexes and the precipitation of salts were considered by means of a mass-action expression using the appropriate formation constants or solubility products. The activity coefficients of all possible simple and complex species were calculated by the extended Debye-Huckel theory using an updated database (Todorov, et al., 2006).

The saturation indices (SI) (eq. 1), calculated under the experimental conditions were used as indicators for possible salt crystallization (Table 7),

$$SI = \lg(IAP/K) \quad (1)$$

where IAP is an ion activity product and K is a solubility product.

When the solution is supersaturated with respect to a certain salt ($SI > 0$), it will precipitate; when the solution is undersaturated ($SI < 0$), the salt will not precipitate; the solution and the salt will be in equilibrium when $SI = 0$.

Different calcium, magnesium, sodium and potassium salts can simultaneously co-precipitate in electrolyte SBF systems. Their number depends on the precipitation conditions (Table 7).

In the SBF with pH value of 11.5, nine salts display positive SI, namely $Mg(OH)_2$, $CaHPO_4$, $Mg_3(PO_4)_2 \cdot 8H_2O$, $MgCO_3 \cdot Mg(OH)_2 \cdot 3H_2O$, $CaCO_3$, $Ca_3(PO_4)_2(am)$, $Ca_8H_2(PO_4)_6 \cdot 5H_2O$, $Ca_9Mg(HPO_4)(PO_4)_6$ and $Ca_{10}(PO_4)_6(OH)_2$ (Table 7) and can co-precipitate. At pH 8 the same salts including $CaHPO_4 \cdot 2H_2O$ but except $Mg(OH)_2$ can co-precipitate. The increase of the Mg^{2+} ion concentration in the system leads to co-precipitation of extra four metastable magnesium salts and favors the precipitation of $Ca_9Mg(HPO_4)(PO_4)_6$ (SI increases). The increase of the Zn^{2+} concentration in the system does not influence the co-precipitated salts. The only zinc phosphate salt $Zn_3(PO_4)_2 \cdot 4H_2O$ is not expected to precipitate ($SI < 0$). In SBF of pH 6 where DCPD precipitates, only calcium phosphate salts can co-precipitate. In all cases, the highest SI and the highest thermodynamic stability are displayed by $Ca_{10}(PO_4)_6(OH)_2$ followed by $Ca_9Mg(HPO_4)(PO_4)_6$. Despite the thermodynamic stability of HA, the kinetic factors favor the formation of metastable phases - ACP at pH 8 and 11.5 and initial $(Ca+Me)/P = 1.67$ and DCPD at pH 6 and $Ca/P = 1$. These results are in compliance with Ostwald's step rule, according to which the crystal phase that nucleates is not the phase that is most thermodynamically stable under these conditions, but rather is a metastable phase closest in free energy to the parent phase (Chung, et al., 2009). The highest crystallization rate and the lowest supersaturation necessary for nucleation should be exhibited by those salts in the saturated solution, for which there is a sufficient concentration of structural entities able to be incorporated unchanged or with small changes into the crystal structure.

5. Biomimetic modifications and phase transformations of ACP and DCPD

With the aim to elucidate the influence of micro-environmental surroundings on the phase transformation process of SBF-modified ACP, DCPD, and Zn-modified ACP we have investigated their biomimetic maturation in SBFs by means of kinetic, spectral and thermodynamic studies. The experiments were performed with three different SBFs -

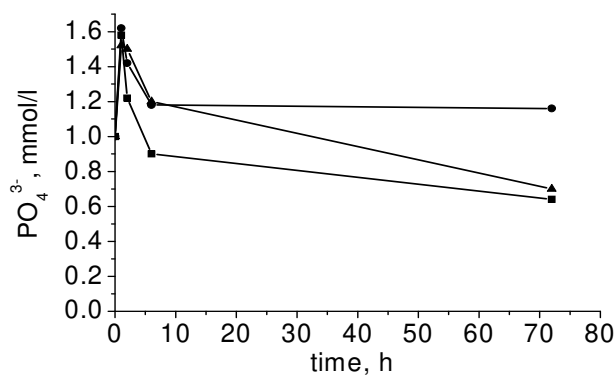
Solid phases	SBF modified ACP		Mg modified ACP	Zn modified ACP	SBF modified DCPD
	pH 11.5	pH 8	pH 8	pH 8	pH 6
NaCl	-3.13	-3.18	-3.14	-3.21	-3.29
NaHCO ₃	-5.75	-3.30	-3.31	-3.24	-3.69
Na ₂ CO ₃ .H ₂ O	-6.78	-7.85	-7.82	-7.77	-10.17
Na ₂ CO ₃ .10H ₂ O	-4.9	-5.97	-5.94	-5.87	-8.80
NaHCO ₃ .Na ₂ CO ₃ .2H ₂ O	-11.65	-10.27	-10.25	-10.13	-12.44
Na ₂ SO ₄	-6.81	-6.80	-6.82	-6.70	-6.70
Na ₂ SO ₄ .10H ₂ O	-5.45	-5.44	-5.46	-5.33	-5.92
KMgPO ₄ .6H ₂ O	-0.32	-0.76	0.60	-1.11	-3.32
Mg(OH) ₂	0.11	-6.63	-5.18	-6.47	-10.95
MgCO ₃	-0.73	-1.50	-0.11	-1.32	-3.98
MgCO ₃ .3H ₂ O	-3.54	-4.31	-2.92	-4.13	-6.49
Mg ₅ (CO ₃) ₄ (OH) ₂ .4H ₂ O	-5.12	-14.94	-7.91	-14.07	-27.17
MgCO ₃ .Mg(OH) ₂ .3H ₂ O	1.09	-6.42	-3.57	-6.08	-12.29
MgSO ₄ .7H ₂ O	-6.47	-6.16	-4.81	-5.96	-6.13
MgHPO ₄ .3H ₂ O	-3.49	-0.38	0.95	-0.60	-0.76
Mg ₃ (PO ₄) ₂	-1.08	-1.60	2.5	-1.90	-6.72
Mg ₃ (PO ₄) ₂ .8H ₂ O	0.78	0.27	4.36	-0.03	-4.86
Mg ₃ (PO ₄) ₂ .22H ₂ O	-1.23	-1.74	2.35	-2.02	-6.85
Ca(OH) ₂	-1.39	-8.52	-8.45	-8.54	-12.06
CaCO ₃	2.62	1.45	1.46	1.46	-0.87
CaSO ₄	-1.67	-1.76	-1.80	-1.74	-1.67
CaSO ₄ .2H ₂ O	-1.44	-1.53	-1.56	-1.50	-1.49
CaHPO ₄	0.14	2.86	2.86	2.86	2.20
CaHPO ₄ .2H ₂ O	-0.15	2.56	2.51	2.17	1.96
Ca ₃ (PO ₄) ₂ (am)	8.37	6.66	6.62	5.85	1.35
Ca ₈ H ₂ (PO ₄) ₆ .5H ₂ O	26.63	28.64	28.45	26.24	17.14
Ca ₉ Mg(HPO ₄)(PO ₄) ₆	34.19	32.19	33.39	29.54	15.88
Ca ₁₀ (PO ₄) ₆ (OH) ₂	60.18	47.92	47.87	45.49	28.35
Zn(OH) ₂				-6.44	
ZnCO ₃				-5.35	

$\text{ZnCO}_3 \cdot \text{H}_2\text{O}$				-5.10	
$\text{Zn}_2(\text{OH})_3\text{Cl}$				-12.28	
$\text{ZnSO}_4 \cdot \text{H}_2\text{O}$				-13.98	
$\text{ZnSO}_4 \cdot 6\text{H}_2\text{O}$				-12.88	
$\text{ZnSO}_4 \cdot 7\text{H}_2\text{O}$				-12.64	
$\text{Zn}_2(\text{OH})_2\text{SO}_4$				-16.36	
$\text{Zn}_3(\text{PO}_4)_2 \cdot 4\text{H}_2\text{O}$				-9.49	

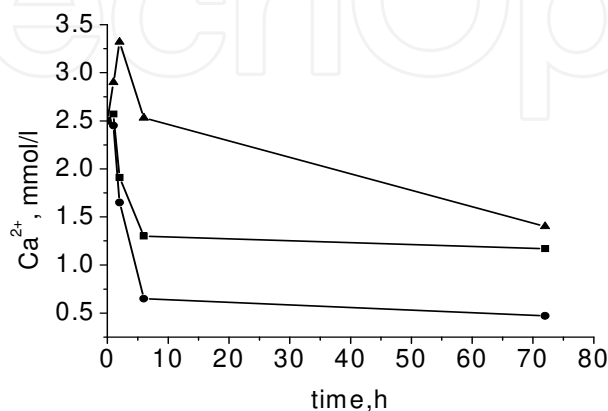
Table 7. Saturation indices (SI) of solid phases in the studied systems.

conventional, SBFc, revised, SBFr, and conventional modified with glycine, SBFg (Table 3). Before maturation the precipitated precursors were filtered, washed with water and with acetone (solid-to-liquid ratio of 1:1) and lyophilized at -56°C . Then the freeze-dried samples were matured for varying time periods (from 1 h to 6 months) at a solid-to-liquid ratio of 1:250, physiological temperature of 37°C , in a static regime.

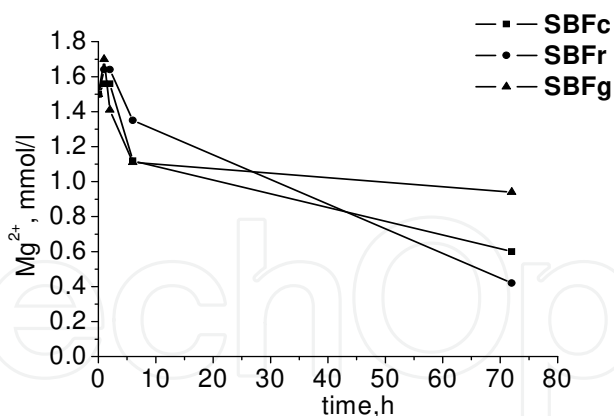
The biomimetic modification of SBF-modified ACP in SBFc, SBFr and SBFg gave rise to changes in the compositions of both solid and liquid phases during the maturation process (Fig. 3) and revealed that dissolution/crystallization processes are strongly influenced by the content of SBFs.



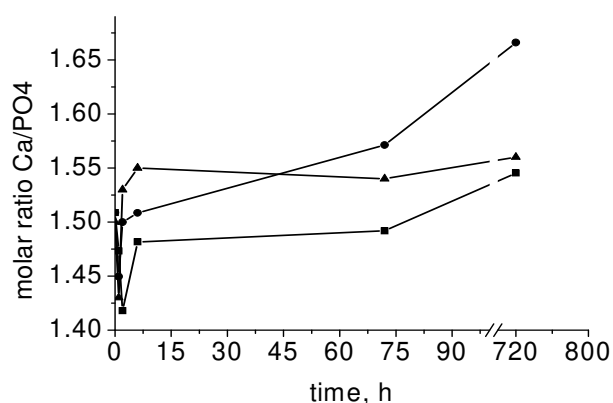
a.



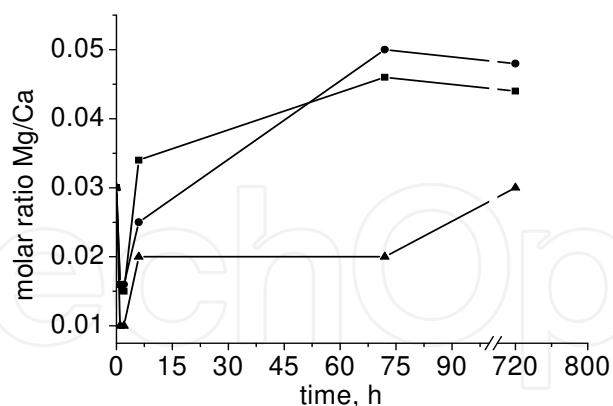
b.



c.



d.



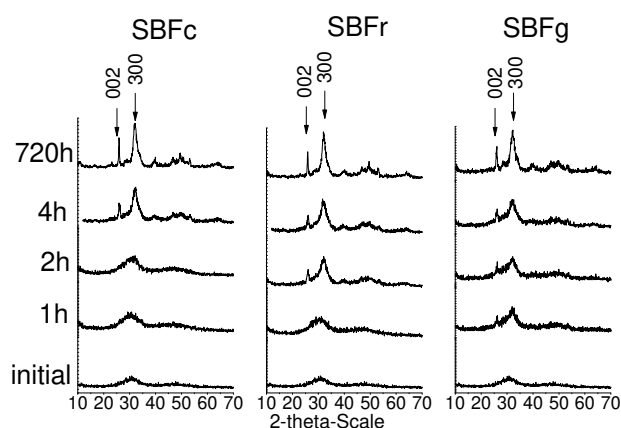
e.

Fig. 3. Kinetic profiles of PO_4^{3-} (a), Ca^{2+} (b) and Mg^{2+} (c) in liquid and solid (d, e) phases.

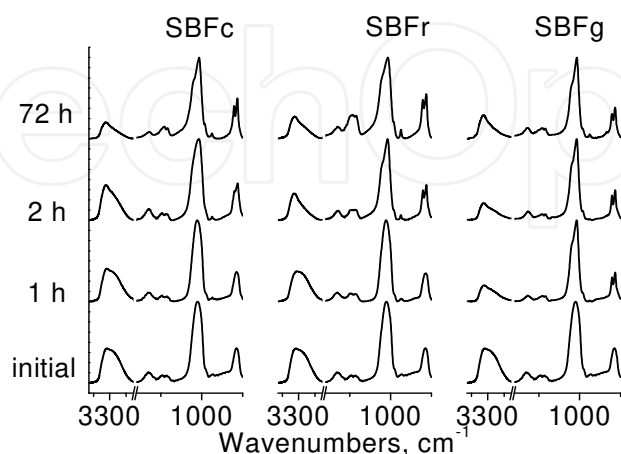
A similar behavior of PO_4^{3-} (Fig. 3a), Ca^{2+} (Fig. 3b), and Mg^{2+} (Fig. 3c) ions was found in the three SBFs. The biggest changes were registered during the first 6 hours. The liquid phases were enriched in Ca^{2+} , Mg^{2+} , and PO_4^{3-} ions during the first 2 - 4 h; afterwards, until the 6th hour, the enrichment rate gradually decreased. The highest increase was registered for Ca^{2+} (32%) and Mg^{2+} (46%) ions in SBFg. Their highest decrease was observed in SBFr. For Ca^{2+}

ions this decrease was about 90% for 6 hours, while for Mg^{2+} ions the decrease continued after the 6th hour and reached 83% at the 72nd hour. The presence of glycine in SBFg and the higher content of HCO_3^- ions in SBFr leads to formation of metal-glycine and metal-carbonate complexes that enhance the solubility of the salts. During maturation in SBFr which is richer in HCO_3^- , crystallization of $CaCO_3$ occurs, also confirmed by the increased Ca/P ratios in the solid phase (Fig.3d), whereas in SBFc and SBFg the formation of calcium phosphate dominates. The increase of the Mg/Ca ratio in the solid phases (Fig.3e) gives an evidence for the incorporation of Mg^{2+} in the amorphous phase.

The spectral studies (XRD and IR) confirmed the biomimetic phase transformation of amorphous calcium phosphate into the more stable poorly-crystalline apatite in the three SBFs, differing only in the phase transformation rate (Fig 4). Crystal phase was detected at the 4th hour of the maturation process in SBFc; at the 2nd hour in SBFr and at the 1st hour in SBFg (Fig 4a). The increase in the degree of crystallinity during the maturation process was confirmed by the observed splitting of the phosphate bands at 960, 1100, 562, and 603 cm^{-1} , which are characteristic for the IR spectra of crystalline calcium phosphate (Fig 4b).



a.



b.

Fig. 4. XRD patterns (a) and IR (b) spectra for different SBFs and maturation times.

IR data also revealed a change in the carbonate content of the samples treated in SBFc and SBFr with different carbonate content (Fig. 5). As a measure of the carbonate content we used the ratio between the areas underneath the peaks corresponding to CO_3^{2-} ($1549\text{-}1336\text{ cm}^{-1}$) and PO_4^{3-} ($1280\text{-}914\text{ cm}^{-1}$) stretching bands. As can be seen, the amount of carbonate ions faster increases in samples matured in SBFr than in those matured in SBFc. **Thermodynamic modeling** of the maturation process of two different solid calcium phosphate products - a metastable amorphous product (*ACP), and a stable equilibrium product (**ACP) were done in the three solutions (SBFc, SBFr and SBFg) differing in their ionic content (Table 8).

Phase	Maturation of *ACP			Maturation of **ACP		
	SBFc	SBFr	SBFcg	SBFc	SBFr	SBFcg
NaCl	-3.59	-3.66	-3.59	-3.59	-3.65	-3.59
Na ₂ SO ₄	-6.15	-6.14	-6.16	-6.14	-6.13	-6.14
Na ₂ SO ₄ .10H ₂ O	-5.34	-5.32	-5.35	-5.33	-5.31	-5.33
NaHCO ₃	-3.53	-3.17	-3.59	-3.81	-2.4	-3.54
NaHCO ₃ .Na ₂ CO ₃ .2H ₂ O	-9.76	-8.69	-9.94	-12.95	-9.05	-12.04
Na ₂ CO ₃ .H ₂ O	-7.66	-6.94	-7.78	-10.56	-8.08	-9.93
Na ₂ CO ₃ .10H ₂ O	-6.25	-5.53	-6.37	-9.15	-6.67	-8.53
MgSO ₄ .7H ₂ O	-5.26	-5.84	-5.33	-5.25	-5.25	-5.22
MgCO ₃	-1.17	-1.05	-1.34	-4.07	-1.6	-3.40
MgCO ₃ .3H ₂ O	-3.67	-3.55	-3.84	-6.56	-4.1	-5.90
Mg ₃ (PO ₄) ₂	-2.27	-1.90	-2.78	-9.29	-5.77	-8.00
MgHPO ₄ .3H ₂ O	-1.01	-0.89	-1.19	-1.91	-1.21	-1.64
Mg ₃ (PO ₄) ₂ .22H ₂ O	-2.3	-1.93	-2.83	-9.32	-5.8	-8.06
Mg ₅ (CO ₃) ₄ (OH) ₂ .4H ₂ O	-10.95	-10.33	-11.80	-27.75	-15.76	-24.36
KMgPO ₄ .6H ₂ O	-2.92	-2.43	-3.25	-6.43	-4.66	-5.91
Ca(OH) ₂	-9.01	-9.01	-9.01	-14.34	-13.49	-14.06
CaSO ₄	-2.77	-3.48	-2.66	-2.86	-4.13	-3.29
CaSO ₄ .2H ₂ O	-2.58	-3.28	-2.48	-2.67	-3.94	-3.10
CaMg ₃ (CO ₃) ₄	-3.18	-2.81	-3.69	-14.86	-6.25	-12.67
CaHPO ₄ .2H ₂ O	-0.23	-0.23	-0.23	-1.23	-1.8	-1.42
Mg(OH) ₂	-5.95	-5.93	-6.16	-11.05	-9.0	-10.47
Mg ₃ (PO ₄) ₂ .8H ₂ O	-0.37	0	-0.89	-7.14	-3.77	-6.16
MgCO ₃ .Mg(OH) ₂ .3H ₂ O	-4.41	-4.27	-4.83	-12.29	-7.75	-11.12
CaCO ₃	0	0	0	-2.94	-1.77	-2.80
CaHPO ₄	0	0	0	-1.05	-1.61	-1.11
Ca ₃ (PO ₄) ₂ (am)	0	-0.10	0	-6.76	-7.64	-7.43
Ca ₈ H ₂ (PO ₄) ₆ .5H ₂ O				-6.62	-8.43	-7.19
Ca ₉ Mg(HPO ₄)(PO ₄) ₆				-11.37	-11.55	-11.36
Ca ₁₀ (PO ₄) ₆ (OH) ₂				0	0	0

Notes: The impurities in the washed initial products were taken in the range 1-3 % based on the measured Mg/Ca ratio (3 mol %) (Table 5).

*ACP - metastable amorphous product; **ACP - stable equilibrium product.

Table 8. Likely salts in the biomimetic systems and their thermodynamic calculated saturated indices (SI) at biomimetic maturation.

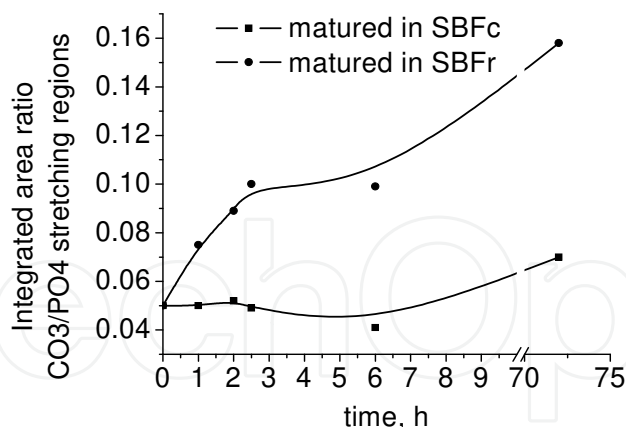


Fig. 5. Changes in the carbonate content of the samples treated in SBFc and SBFr.

The metastable amorphous product (*ACP) simulated the system behavior during the first 1-2 hours of maturation, when no $\text{Ca}_8\text{H}_2(\text{PO}_4)_6 \cdot 5\text{H}_2\text{O}$, $\text{Ca}_9\text{Mg}(\text{HPO}_4)(\text{PO}_4)_6$ and $\text{Ca}_{10}(\text{PO}_4)_6(\text{OH})_2$ phase was yet formed, whereas the stable product (**ACP) simulated the equilibrium system. The maturation of the metastable amorphous product (*ACP) leads to a phase transformation that depends on the content of HCO_3^- ions in SBF at the beginning of the process (Table 8). In a solution with a low HCO_3^- content (SBFc and SBFg), dissolution phenomena of all magnesium salts occur ($\text{SI} < 0$) during maturation and the system will be in equilibrium with the calcium salts ($\text{SI} = 0$), including the amorphous calcium phosphate. The increase in the HCO_3^- content (SBFr) leads to dissolution and phase transformation of the amorphous calcium phosphate into thermodynamically more stable salts. The calculated equilibrium amounts of CaCO_3 and $\text{Ca}_3(\text{PO}_4)_2(\text{am})$ in the three investigated body fluids (Fig. 6) point to the significantly favored crystallization of CaCO_3 (especially in SBFr) and the decreased amount of $\text{Ca}_3(\text{PO}_4)_2(\text{am})$ due to dissolution processes. The calculations revealed that there was no influence of SBFs composition on the equilibrium product (**ACP), the system tending to thermodynamic equilibrium by dissolution of all co-precipitated solid phases and re-crystallization of the thermodynamically unstable amorphous calcium phosphate (with $\text{SI} < 0$) into pure HA (with $\text{SI} = 0$) (Table 8).

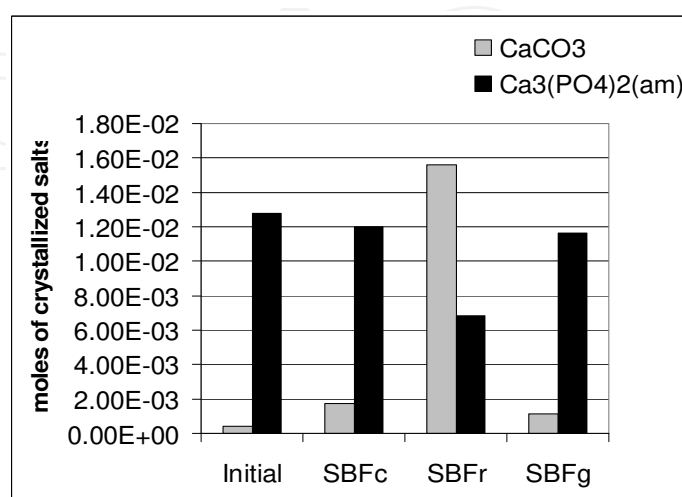


Fig. 6. Calculated equilibrium amounts of CaCO_3 and $\text{Ca}_2(\text{PO}_4)_3(\text{am})$.

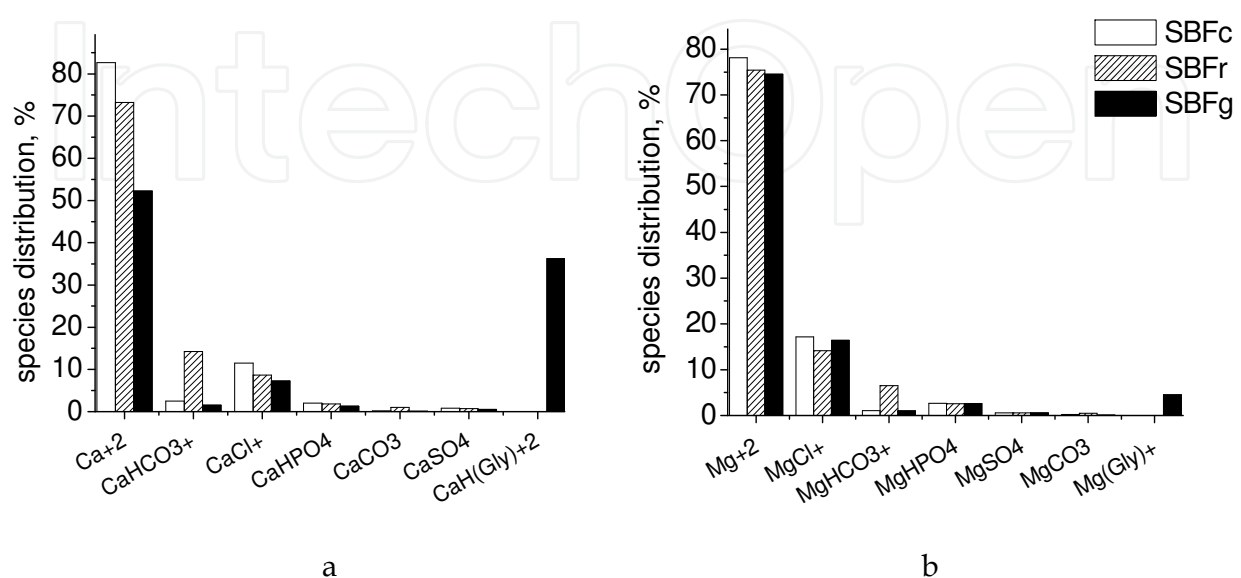
The model cannot predict the formation of Mg-substituted carbonated hydroxyapatite due to the lack of thermodynamic data.

The calculated species distribution in the initial SBFs, in the SBFs at metastable (maturation of *ACP) and at stable (maturation of **ACP) equilibrium (Fig. 7) gives an evidence for the domination of Me^{2+} ($\text{Me} = \text{Ca}, \text{Mg}$) free ions in all studied cases. In the initial SBFs (Fig. 7a and 7b) and at a stable thermodynamic equilibrium (Fig. 7e and 7f) Me^{2+} free ions are dominating, followed by MeCl^+ in SBFc, from MeHCO_3^- and MeCl^+ in SBFr and from $\text{CaH}(\text{Gly})^{2+}$ and CaCl^+ and from MgCl^+ and $\text{Mg}(\text{Gly})^+$ in SBFg. Significant changes in species distribution are observed at a metastable equilibrium (Fig. 7c and 7d), revealing the essential role of SBF ionic composition on the maturation process. The increased amount of MeHPO_4^{2-} , CaPO_4^- in SBFc and SBFr, as well as the increased amount of $\text{Me}(\text{Gly})^+$ species in SBFg is due to the dissolution of metastable salts while the decreased amount of MeHCO_3^- species especially in SBFr is due to the crystallization of CaCO_3 .

These thermodynamic data explain the results from the maturation kinetics.

The **biomimetic modifications of Zn-modified ACP** were studied on three exemplary samples with different $\text{Zn}^{2+}/(\text{Zn}^{2+} + \text{Ca}^{2+})$ molar ratios (0.03, 0.05 and 0.10), treated in a conventional simulated body fluid (SBFc). It was found that the Zn content decreases by a factor of 2 during the first 2 hours (Fig. 8) when the samples are still amorphous (Fig. 9). Subsequently, the amorphous phase progressively converted into poorly-crystalline apatite. The Zn content influenced the transformation rate. At a higher Zn content the stability of the amorphous phase increased and the rate of the process slowed down (Fig. 9).

The kinetic studies of the **biomimetic modifications of DCPD** revealed that the compositions of the liquid and solid phases, similar to those of ACP, changed during the maturation process (Fig. 10). In SBFg the highest increase in PO_4^{3-} and Ca^{2+} concentrations was registered as a result of the effect of glycine which promotes the dissolution of DCPD. In the solid phase the Ca/PO_4 ratio is kept ≈ 1 during the first 6 hours, then gradually increases. The latter is an indication for the beginning of the transformation process and the formation of basic calcium phosphates with $\text{Ca}/\text{PO}_4 > 1$.



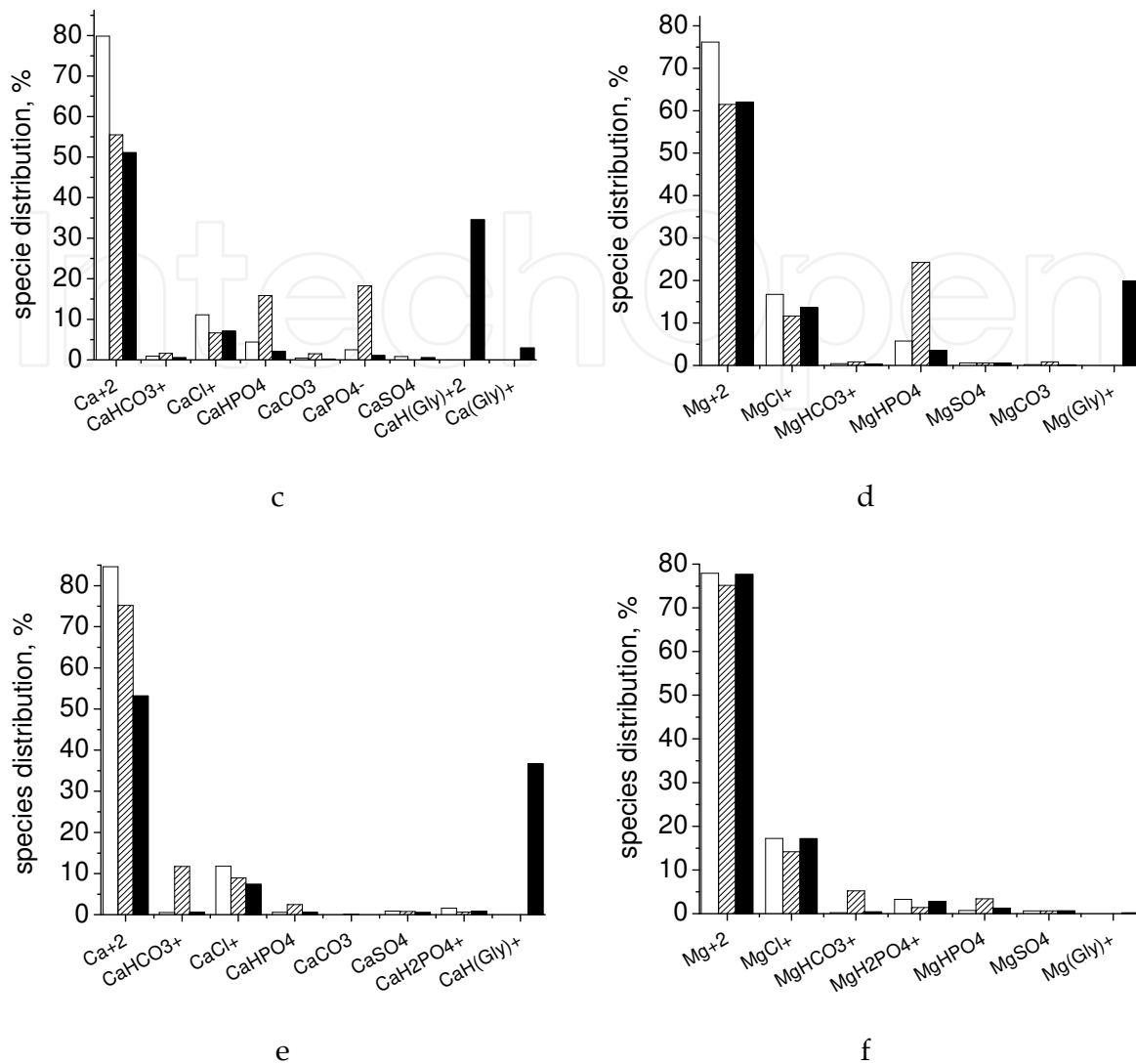


Fig. 7. Ca and Mg species distribution in initial SBF (a and b); at maturation of *ACP (c and d); at maturation of **ACP (e and f)

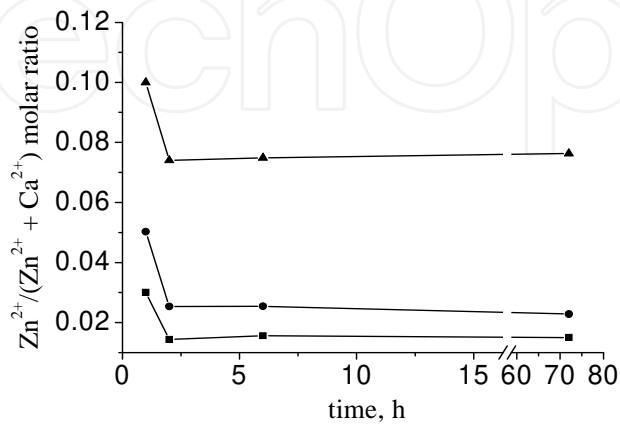


Fig 8. Time dependence of the solid phase $Zn^{2+}/(Zn^{2+} + Ca^{2+})$ molar ratio during maturation.

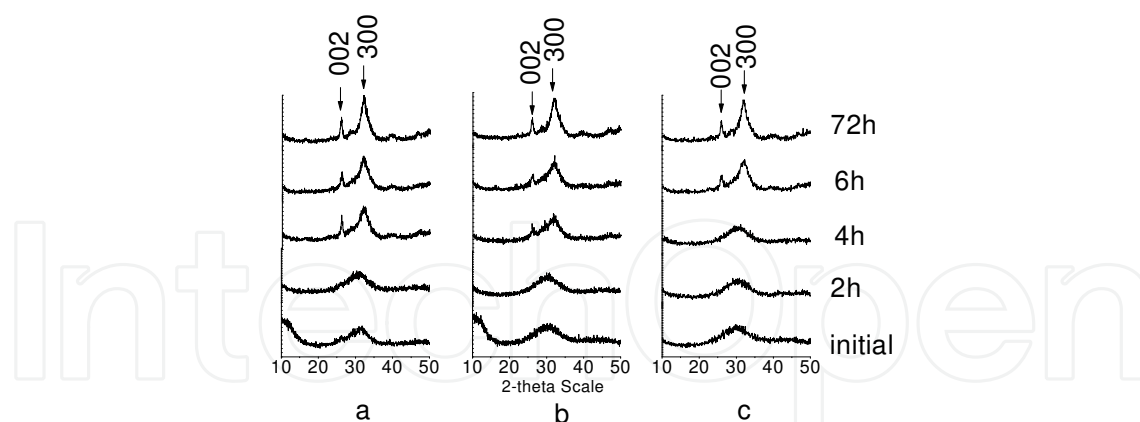


Fig. 9. XRD patterns of solid phases with Zn²⁺/(Zn²⁺ + Ca²⁺) ratios of 0.03 (a); 0.05 (b) and 0.1 (c) matured for different times in SBFc.

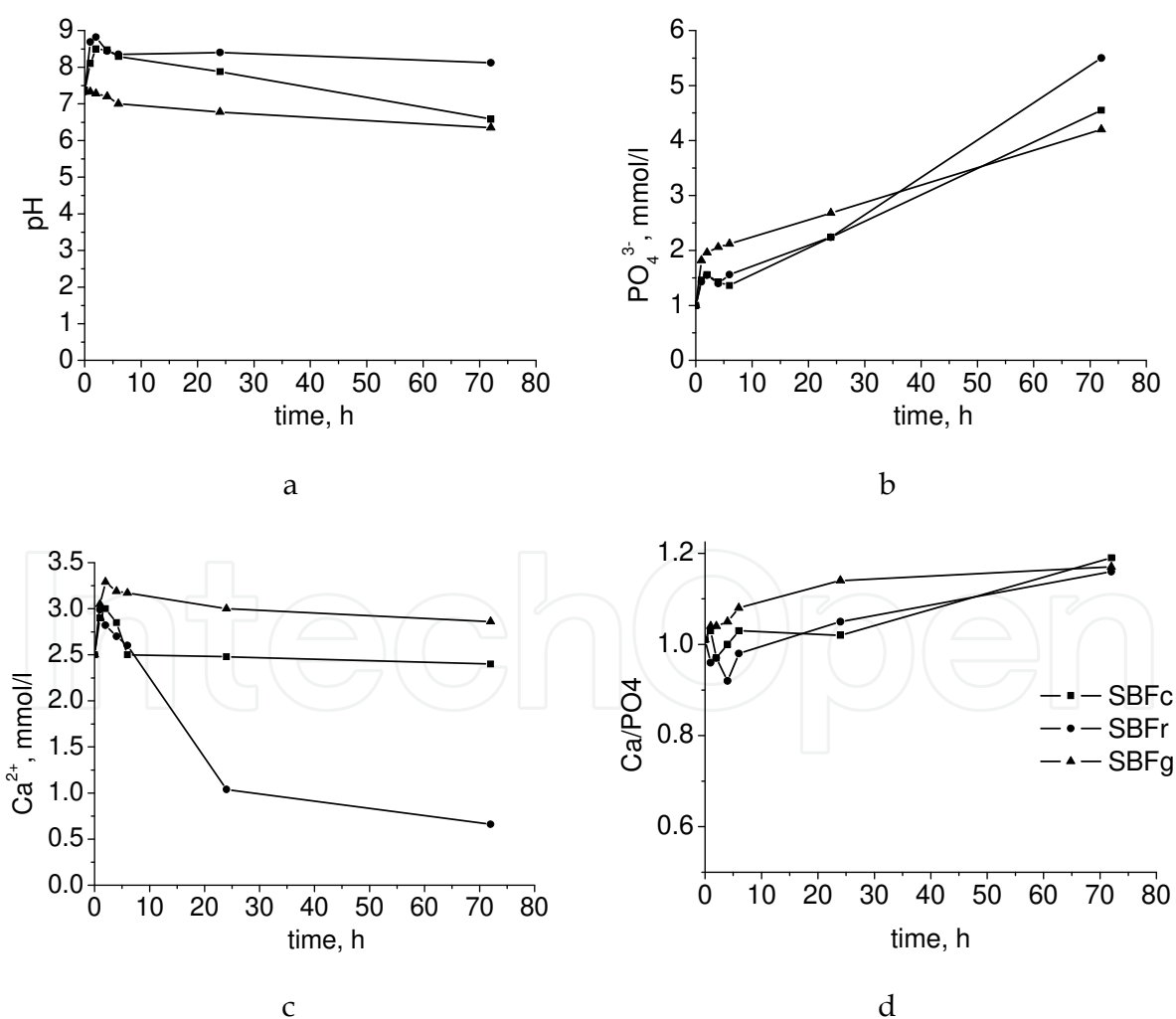
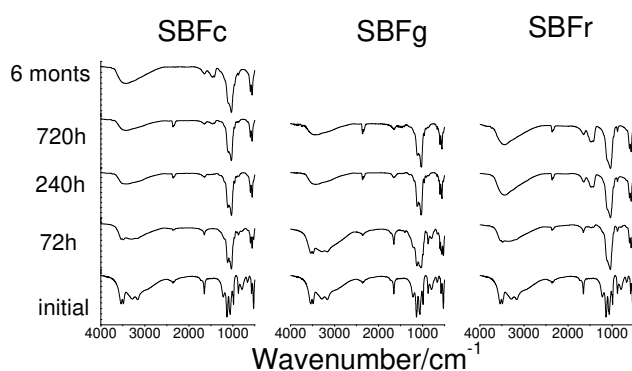
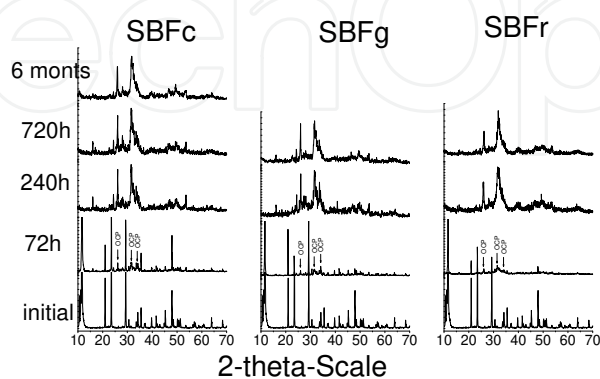


Fig. 10. Kinetic profiles of pH (a), PO₄³⁻ (b), Ca²⁺ (c), in the liquid phases and of the Ca/PO₄ ratio in the solid phases (d) during maturation.

IR and XRD data (Fig.11) show that the initial DCPD transforms into poorly-crystalline B-type carbonate apatite via an intermediate phase of OCP. The rate of conversion of DCPD to carbonated apatite differs, depending on the type of SBF. The formation of carbonated apatite is faster in SBFr, as it is indicated by the disappearance of O-H and P-OH peaks typical of DCPD phase and the appearance of absorption bands near 1420 and 1480 cm^{-1} associated with B-type CO_3^{2-} groups after 240 h of treatment (Rabadjieva et al., 2010). For samples treated in SBFc DCPD phase is still preserved after 72 h of treatment, while the carbonate peaks appeared after 720h (one month) maturation and increased in intensity after 6 months, indicating slow rate of PO_4^{3-} substitution by CO_3^{2-} groups. Intense absorption bands in the 1073-1122 cm^{-1} spectral range are due to the asymmetric stretching vibration mode of P-O, whereas the absorption band that appears near 963 cm^{-1} is associated with the symmetric stretching mode of P-O. Peaks at 602, 562 and at 470 cm^{-1} originate from O-P-O bending modes. O-H stretching bands of crystalline water appeared in the range of 3500-3100 cm^{-1} , while H_2O bending is at 1640-1650 cm^{-1} . Peaks at 1297 and 1192 cm^{-1} are due to the P-OH bending mode of HPO_4^{2-} groups, while those near 914 and 870 cm^{-1} arise from the stretching mode of HPO_4^{2-} groups and partially overlapped with C-O vibrations. The absorption bands at around 878 cm^{-1} could be due to bending vibration of CO_3^{2-} groups, because are related with intensive bands in the 1400-1500 cm^{-1} spectral interval, typical of C-O stretching vibrations. Peak at 526 cm^{-1} is associated with HO- PO_3 bending mode in HPO_4^{2-} (Mendel & Tas, 2010; LeGeros et al., 1989).



a.

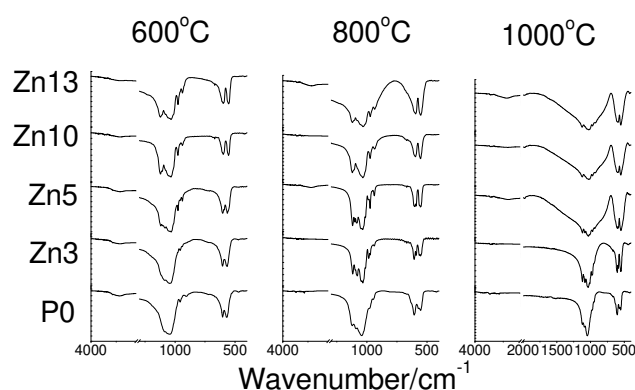


b.

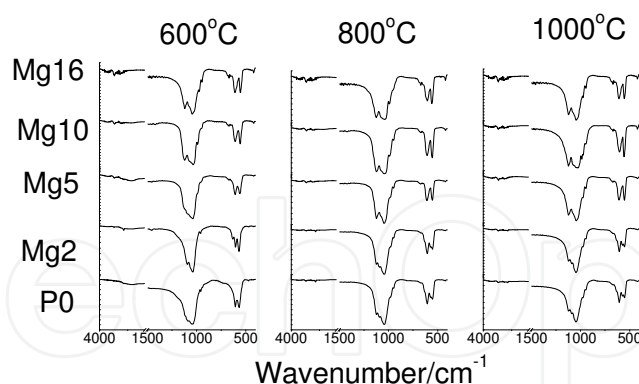
Fig. 11. IR spectra (a) and XRD patterns (b) at different maturation time.

6. High-temperature phase transformations of ion modified ACP

The matured Zn- and Mg-modified ACP precursors were treated by a procedure including gelation with Xanthan gum, lyophilization at -56°C , washing (solid-to-water ratio of 1:100) and secondary lyophilization. Then they were sintered at 600, 800 and 1000°C in order to study the high-temperature phase transformations and to follow the effect of Mg^{2+} and Zn^{2+} on the Ca^{2+} ion substitution and on the phase composition and morphology of the sintered products. The working regime consisted of heating at a rate of $3^{\circ}\text{C}/\text{min}$ up to the desired temperature and keeping it constant for 1 hour. Both, concentration of Mg^{2+} and Zn^{2+} ions and temperature affect the spectral characteristics of the studied samples (Fig. 12). The hydroxyl stretching peaks near 3570 cm^{-1} and the hydroxyl librations at 633 cm^{-1} revealed the presence of HA phase, while the peaks near 1120, 1075, 1040, 975 and 950 cm^{-1} indicated the formation of β -TCP phase.



a.

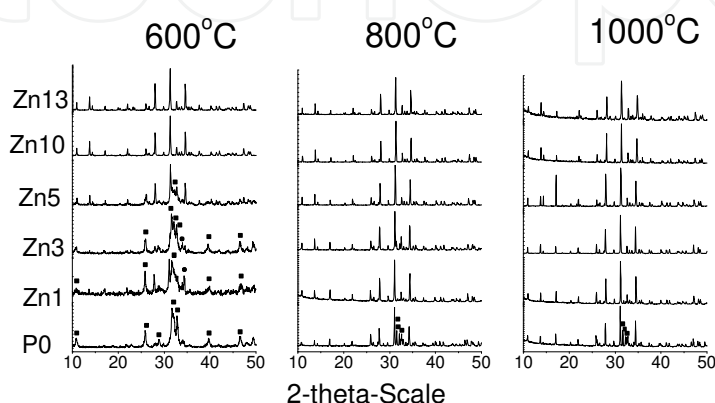


b.

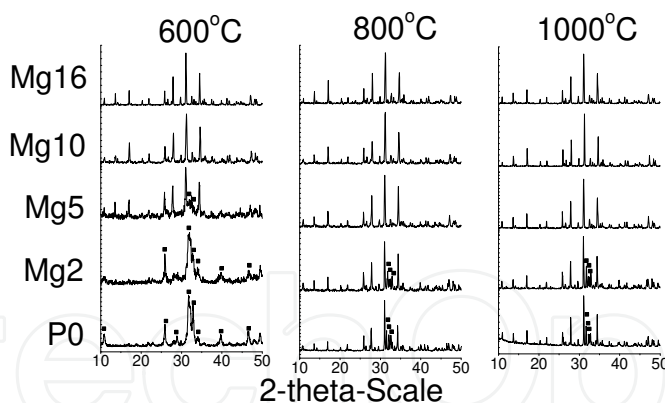
Fig. 12. FT IR spectra of Zn-modified (a) and Mg-modified (b) calcium phosphates at different temperatures.

The XRD data (Fig. 13) revealed that all amorphous precursors were transformed into ion-modified HA or β -TCP crystalline phases depending on the additive and its amount as well as on the temperature. Both Zn and Mg substitutions promoted the ACP transformation to ion-modified HA and β -TCP but the effect was more pronounced in the case of Zn substitution. Zn- β -TCP and Mg- β -TCP were registered at 600°C for samples with

$Me^{2+}/(Me^{2+} + Ca^{2+})$ ratios higher than 0.05 and mixture of the ion-modified HA and β -TCP calcium phosphates at ratios lower than 0.05. The SEM analyses revealed that Zn and Mg substitutions influenced the morphology of the β -TCP grains (Fig 14). Sintering at 800-1000°C leads to zinc-modified- β -TCP powders of idiomorphic crystals with sizes ranging from 500 to 5000 nm in all studied cases. Magnesium-modified- β -TCP fine powders with spherical grains of smaller size (250 - 1000 nm) were obtained at a $Mg^{2+}/(Mg^{2+} + Ca^{2+})$ ratio higher than 0.02 (Figure 13 and 14). The surface of the spherical grains of magnesium modified samples was covered by blanket, while clean grain boundary was observed in the zinc-modified samples.



a.



b.

Fig. 13. XRD powder data of Zn-modified (a) and Mg-modified (b) calcium phosphates at different temperatures. (■ - HAP; not marked - Me^{2+} - β -TCP).

The calculated unit cell parameters showed that low ion substitution ($Me^{2+}/(Me^{2+}+Ca^{2+})$ ratio up to 0.05) leads to a slight decrease in the parameter **a** and the volume **V** and to an increase in the parameter **c** of the Me - β -TCP unit cell (Table 9). This tendency became more pronounced at higher temperatures.

The inclusion of Mg^{2+} and Zn^{2+} ions into the crystal unit cell of the thermodynamically stable HA proceeds through Ca^{2+} ion substitution. As the ionic radii of Mg^{2+} (0.65 Å) and

Sample	600°C			800°C			1000°C		
	a, Å	c, Å	V, Å ³	a, Å	c, Å	V, Å ³	a, Å	c, Å	V, Å ³
Zinc-modified calcium phosphates									
Zn1	*	*	*	10.423	37.339	3513	10.417	37.393	3514
Zn3	*	*	*	10.437	37.101	3500	10.390	37.142	3471
Zn5	*	*	*	10.397	37.062	3469	10.387	37.042	3460
Zn10	10.345	36.902	3420	10.329	36.903	3410	10.349	37.153	3446
Zn13	10.332	37.005	3421	10.349	36.988	3431	10.339	37.227	3446
Magnesium-modified calcium phosphates									
Mg2	*	*	*	10.420	37.278	3505	10.415	37.301	3504
Mg5	10.419	37.314	3508	10.403	37.324	3498	10.393	37.319	3491
Mg10	10.356	37.161	3452	10.368	37.234	3466	10.346	37.134	3442
Mg16	10.332	37.152	3435	10.340	37.213	3446	10.391	37.28	3486

* poorly crystallized phase.

Table 9. Unit cell parameters of Me²⁺-modified calcium phosphates.

Zn²⁺ (0.74 Å) are too small in comparison with that of Ca²⁺ (1.00 Å) the increase in their amount leads to unit cell distortion and volume decrease, established also by Ito et al. (2002) and Miyaji et al. (2005). Thus, the structure of Me²⁺ ion modified HA is destabilized and

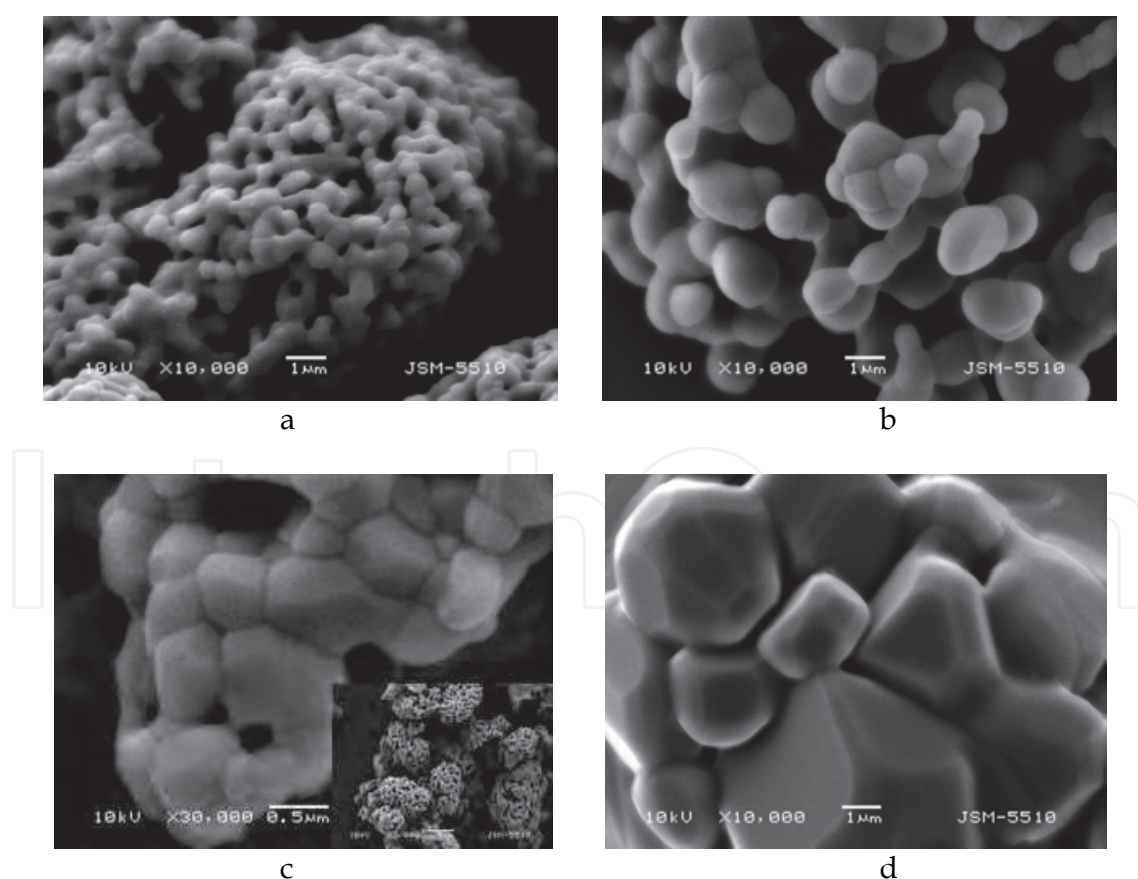


Fig. 14. SEM images of Me²⁺-modified calcium phosphates heated at 1000°C: a) Mg²⁺/(Mg²⁺+Ca²⁺) = 0.02; b) Mg²⁺/(Mg²⁺+Ca²⁺) = 0.10; c) Zn²⁺/(Zn²⁺+Ca²⁺) = 0.01; d) Zn²⁺/(Zn²⁺+Ca²⁺) = 0.13.

its transformation into the more stable β -TCP structure could be expected. The latter structure includes different CaO_n coordination polyhedra ($n=3,6,7,8$) (Yashima et al., 2003). The vacant sites of the smallest CaO_3 polyhedron are the most suitable holes for the inclusion of the small Mg^{2+} and Zn^{2+} ions, thus the unit cell distortion and structure destabilization will be negligible. Ion substitution at a $\text{Me}^{2+}/(\text{Ca}^{2+}+\text{Me}^{2+})$ ratio higher than 0.05-0.15 leads to an increase in the Me^{2+} ion inclusion into the larger CaO_n polyhedra ($n=6-8$), which destabilizes the structure. The appearance of a more stable high-temperature modification, α -TCP, could be expected in this case, but no α -TCP XRD peaks were detected in our experiments.

7. Conclusions

In a summary, original authors' studies and literature data are presented on the biomimetic synthesis of XRD-amorphous calcium phosphate and dicalcium phosphate dihydrate and their biomimetic modifications and phase transformations into poorly-crystalline apatite in three types of simulated body fluids - conventional (SBFc), revised (SBFr) and modified with glycine (SBFg). The compositions of the different types of artificial body fluids that are known in the literature are compared in terms of their similarity to blood plasma; their advantages and disadvantages are highlighted. The authors' studies and original results on chemical and phase compositions, kinetics and thermodynamic simulations are discussed. A new approach based on thermodynamic modeling (using the PHREEQCI v.2.14.3 computer program based on an ion-association model) was applied for simulation and explanation of the biomimetic precipitation of metastable XRD-amorphous calcium phosphate and dicalcium phosphate dihydrate instead of the thermodynamically stable hydroxyapatite and of their biomimetic phase transformations during the maturation processes. The crucial role of the SBF as an electrolyte system is emphasized.

8. Acknowledgements

This work is financially supported by the Bulgarian Ministry of Education, Youth and Science under Projects DTK 02-70/2009 and CVP-09-0003.

9. References

- Bassett, H. (1917) The phosphates of calcium. Part IV. The basic phosphates. *J. Chem. Soc. Trans.*, Vol. 111, pp. 620-642. DOI: 10.1039/CT9171100620
- Bassett, H. (1958). The Phosphates of Calcium, Part V. Revision of the Earlier Space Diagram. *J. Chem. Soc.*, pp. 2949 - 2955, DOI: 10.1039/JR9580002949
- Bayraktar, D. & Tas, A.C. (1999) Chemical preparation of carbonated calcium hydroxyapatite powders at 37°C in urea-containing synthetic body fluids. *J Eur Ceram Soc*, Vol. 19, pp. 2573-2579, ISSN 0955-2219
- Belopol'skii, A.P.; Serebrennikova, M.T. & Belevich, A.V. (1940) Vapour Pressure of Saturated Solutions and Solubilities in the System $\text{CaO-P}_2\text{O}_5\text{-H}_2\text{O}$ (In Russian). *Zhurnal Prikl. Khim.*, Vol. 13, No 1, pp. 3-10. C.A. 34:7718¹

- Betts, F.; Blumenthal, N.C.; Posner, A.S.; Becker, G.L. & Lehninger, A.L. (1975) Atomic Structure of Intracellular Amorphous Calcium Phosphate Deposits. *Proc Natl Acad Sci USA*, Vol. 72, pp. 2088-2092, ISSN 1091-6490.
- Bigi, A.; Foresti, E.; Gandolfi, M.; Gazzano, M. & Roveri, N. (1995) Inhibiting Effect of Zinc on Hydroxylapatite Crystallization, *Journal of Inorganic Biochemistry*. Vol. 58, pp. 49-58, ISSN 0162-0134
- Blumenthal, N.C.; Betts, F. & Posner, A.S. (1977) Stabilization of Amorphous Calcium Phosphate by Mg and ATP. *Calcif Tissue Res.*, Vol. 23, pp. 245-50, ISSN 0008-0594
- Chepelevskii, M.L.; Bol'ts, Ts.S.; Vasilenko, N.A. & Rubinova, S.S. (1955) Solubility and Rate of Dehydration of $\text{CaHPO}_4 \cdot 2\text{H}_2\text{O}$ (In Russian). *Issledovaniya po Priklad. Khim., Akad. Nauk S.S.S.R., Otdel Khim. Nauk.*, pp. 175-183. C.A. 50:46156b
- Chow, L.C. & Eanes, E.D. (2001). *Octacalcium Phosphate*, Karger, ISBN 3-8055-7228-X, Basel, Switzerland
- Chung, S.Y; Kim, Y.M.; Kim, J.G. & Kim, Y.J. (2009) Multiphase transformation and Ostwald's rule of stages during crystallization of a metal phosphate. *Nature Physics*, Vol. 5, pp. 68-73. ISSN 1745-2473
- Combes, C. & Rey, C. (2010) Amorphous calcium phosphates: Synthesis, properties and uses in biomaterials, *Acta Biomaterialia*, Vol. 6, pp. 3362-3378, ISSN 1742-7061.
- Curry, N.A. & Jones, D.W. (1971) Crystal Structure of Brushite, Calcium Hydrogen Orthophosphate Dihydrate: A Neutron-Diffraction Investigation. *J Chem. Soc., (A)*, pp. 3725-3729, DOI 10.1039/J19710003725
- Daculsi, G.; Bouler, J.M. & LeGeros, R.Z. (1997) Adaptive crystal formation in normal and pathological calcifications in synthetic calcium phosphate and related biomaterials. *Int. Rev. Cytology*, Vol. 172, pp. 129-191, ISSN 0074-7696.
- Dickens, B. & Bowen, J.S. (1971) Refinement of the Crystal Structure of $\text{Ca}(\text{H}_2\text{PO}_4)_2 \cdot \text{H}_2\text{O}$. *Acta Crystallogr.*, Vol. B27, pp. 2247-2255, ISSN 1600-5740
- Dickens, B.; Bowen, J.S. & Brown, W.E. (1972) A Refinement of the Crystal Structure of CaHPO_4 (Synthetic Monetite). *Acta Crystallogr.*, Vol. B28, pp. 797 - 806, ISSN 1600-5740
- Dickens, B.; Schroeder L.W. & Brown, W.E. (1974) Crystallographic Studies of the Role of Mg as a Stabilizing Impurity in $\text{b-Ca}_3(\text{PO}_4)_2$. I. The crystal structure of pure $\text{b-Ca}_3(\text{PO}_4)_2$. *J. Solid State Chem*, Vol. 10, pp. 232 - 248, ISSN 0022-4596
- Dorozhkin, S. V. (April 2009). Calcium Orthophosphates in Nature, Biology and Medicine. *Materials*, Vol. 2, (April 2009), pp. 399-498, ISSN 1996-1944
- Earle, W.R.; Schilling, E.L.; Stark, T.H.; Straus, N.P.; Brown, M.F. & Shelton, E. (1943). Production of malignancy in vitro. IV. The mouse fibroblast cultures and changes seen in the living cells. *JNCI*, Vol. 4, pp. 165-212, ISSN 0027-8874
- Fernandez, E.; Gil, F. J.; Ginebra, M. P.; Driessens, F. C. M.; Planell, J. A. & Best, S. M. (1999) Calcium phosphate bone cements for clinical applications Part I: Solution chemistry. *J Mater Sci: Mater Med*, Vol. 10, pp. 169-176, ISSN 0957-4530.
- Flatt, R.; Brunisholz, G. & Dagon, R. (1961) Contribution a l'etude du systeme quinaire Ca^{++} - NH_4^+ - H^+ - NO_3^- - PO_4^{---} - H_2O XXI. Les solutions saturees a 0 et a 50o du systeme quaternaire Ca^{++} - NH_4^+ - H^+ - PO_4^{---} - H_2O . *Helvetica Chimica Acta*, Vol. XLIV, No VII, pp. 2173-2193, ISSN 1522-2675

- Flatt, R.; Brunisholz, G. & Denereaz, A. (1956) Contribution a l'étude du système quinaire $\text{Ca}^{++} - \text{NH}_4^+ - \text{H}^+ - \text{NO}_3^- - \text{PO}_4^{---} - \text{H}_2\text{O}$ XVIII. Le système quaternaire $\text{Ca}^{++} - \text{H}^+ - \text{NO}_3^- - \text{PO}_4^{---} - \text{H}_2\text{O}$. *Helvetica Chimica Acta*, Vol. XXXIX, No II, pp. 473-483, ISSN 1522-2675
- Fowler, B.O. & Kuroda, S. (1986). Changes in Heated and in Laser-Irradiated Human Tooth Enamel and their Probable Effects of Solubility. *Calcif Tissue Int.*, Vol. 38, pp. 197-208, ISSN 0171-967X
- Gregory, T. M.; Moreno, E.C.; Petel, J.M. & Brown, W.E. (1974) Solubility of $\text{b-Ca}_3(\text{PO}_4)_2$ in the System $\text{Ca}(\text{OH})_2 - \text{H}_3\text{PO}_4$ at 5, 15, 25 and 37°C. *J. Res. Nat. Bur. Stand.*, Vol. 78A, pp. 667-674. ISSN 0022-4332
- Gregory, T.M.; Moreno, E.C. & Brown, W.E. (1970) Solubility of $\text{CaHPO}_4 \cdot 2\text{H}_2\text{O}$ in the System $\text{Ca}(\text{OH})_2 - \text{H}_3\text{PO}_4 - \text{H}_2\text{O}$ at 5, 15, 25, 37.5°C. *J Res Natl Bur Stand*, Vol. 74A, pp. 461-475, ISSN 0022-4332
- Hanks, J.H & Wallace, R.E. (1949). Relation of oxygen and temperature in the preservation of tissues by refrigeration. *Proc. Soc. Exp. Biol. Med.*, Vol. 71, pp. 196-200, ISSN 1525-1373
- Hui, W.; Changjian, L. & Ren, H. (2009) Effects of structure and composition of the CaP composite coatings on apatite formation and bioactivity in simulated body fluid. *Applied Surface Science*, Vol. 255, pp. 4074-4081, ISSN 0169-4332
- Ito, A.; Kawamura, H.; Otsuka, M.; Ikeuchi, M.; Ohgushi, H.; Ishikawa, K.; Onuma, K.; Kanzaki, N. & Sogo, Y., Ichinose, N. (2002). Zinc-releasing calcium phosphate for stimulating bone formation. *Materials Science and Engineering*, Vol. C22, pp. 21-25. ISSN 0921-5093
- Jalota, S.; Bhaduri, S.B. & Tas, A.C. (2006). Effect of carbonate content and buffer type on calcium phosphate formation in SBF solutions. *J Mater Sci:Mater Med.*, Vol. 17, pp. 697-707, ISSN 0957-4530.
- Johnsson, M. S-A. & Nancollas, G.H. (1992). The role of Brushite and Octacalcium Phosphate in Apatite Formation. *Critical Reviews in Oral Biology and Medicine*, Vol. 3, No 1/2, pp. 61-82, ISSN 1045 - 4411
- Kay, M.I.; Young, R.A. & Posner, A.S. (1964) Crystal Structure of Hydroxyapatite. *Nature*, Vol. 204, pp. 1050 - 1052, ISSN 0028-0836
- Kirgintzev, A.N.; Trushnikova, L.N. & Lavrent'eva, V.G. (1972). *Solubility of Inorganic Substances in Water (in Russian)*, Khimia, UDK 541.8(083), Leningrad, Russia
- Klopman, G. (1968) Chemical reactivity and the concept of charge- and frontier-controlled reactions. *J. Am. Chem. Soc.*, Vol. 90, No 2 (January, 1968), pp. 223-234, ISSN 0002 - 7863.
- Kokubo, T. (1990). Surface Chemistry of Bioactive Glass-Ceramics. *J Non-Cryst Solids*, Vol. 120, pp. 138 - 151, ISSN: 0022-3093
- Kontonasaki, E.; Zorba, T.; Papadopoulou, L.; Pavlidou, E.; Chatzizavrou, X.; Paraskevopoulos, K. & Koidis, P. (2002) Hydroxy carbonate apatite formation on particulate bioglass in vitro as a function of time, *Cryst Res Technol*, Vol. 37, pp. 1165-1171, ISSN 0232-1300

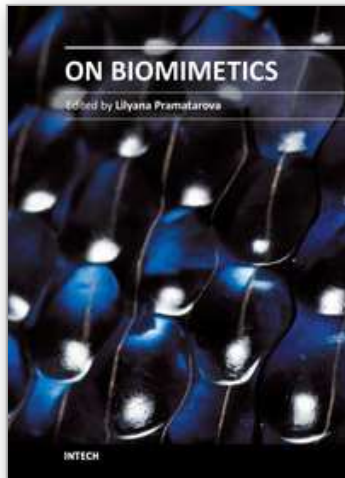
- LeGeros, R.Z.; Daculsi, G.; Orly I, Abergas, T. & Torres, W. (1989) Solution-mediated transformation of octacalcium phosphate (OCP) to apatite. *Scanning Microsc.*, Vol. 3, No 1 (March, 1989), pp. 129-138, ISSN: 0891-7035
- Mandel, S. & Tas A. C. (2010) Brushite ($\text{CaHPO}_4 \cdot 2\text{H}_2\text{O}$) to octacalcium phosphate ($\text{Ca}_8(\text{HPO}_4)_2(\text{PO}_4)_4 \cdot 5\text{H}_2\text{O}$) transformation in DMEM solutions at 36.5 °C. *Materials Science and Engineering*, Vol. C 30, pp. 245–254, ISSN 0921-5093
- Martin, R.A.; Twyman, H.; Qiu, D.; Knowles, J.C. & Newport, R.J. (2009) A study of the formation of amorphous calcium phosphate and hydroxyapatite on melt quenched Bioglass using surface sensitive shallow angle X-ray diffraction. *J Mater Sci: Mater Med*, Vol. 20, pp. 883–888, ISSN 0957-4530.
- Mathew, M. & Takagi, S. (2001). Structures of Biological Minerals in Dental Research. *J. Res. Natl. Inst. Stand. Technol.*, Vol. 106, No 6 (November–December 2001), pp. 1035–1044, ISSN 0160-1741
- Mathew, M.; Brown, W. E.; Schroeder, L. W. & Dickens, B. (1988) Crystal Structure of Octacalcium Bis(Hydrogenphosphate)Tetrakis(Phosphate) Pentahydrate, $\text{Ca}_8(\text{HPO}_4)_2(\text{PO}_4)_4 \cdot 5\text{H}_2\text{O}$. *J. Chem. Crystallogr.*, Vol. 18, pp. 235-250, ISSN 1074-1552
- Mathew, M.; Schroeder, L.W.; Dickens, B. & Brown, W.E. (1977) The crystal Structure of $\alpha\text{-Ca}_3(\text{PO}_4)_2$. *Acta Crystallogr.*, Vol. B33, pp. 1325 – 1333, ISSN 1600-5740.
- Matsuya, S.; Takagi, S. & Chow, L.C. (1996) Hydrolysis of tetracalcium phosphate in H_3PO_4 and KH_2PO_4 . *J. Mater. Sci.*, Vol. 31, pp. 3263-3269, ISSN 0022-2461
- McDowell, H.; Brown, W. E. & Sutter, J. R. (1971). Solubility Study Of Calcium Hydrogen Phosphate. Ion-Pair Formation. *Inorganic Chemistry*. Vol. 10, No. 8, pp. 1638-1643, ISSN 0020-1669.
- McDowell, H.; Gregory, T.M. & Brown W.E. (1977). Solubility of $\text{Ca}_5(\text{PO}_4)_3$ in the System $\text{Ca}(\text{OH})_2 - \text{H}_3\text{PO}_4 - \text{H}_2\text{O}$ at 5, 15, 25 and 37°C. *J. Res. Nat. Bur. Stand.*, Vol. 81A, pp. 273-281, ISSN 0022-4332
- Meyer, J. L. & Eanes, D. E. (1978) A Thermodynamic Analysis of the Secondary Transition in the Spontaneous Precipitation of Calcium Phosphate. *Calcif. Tissue Res.*, Vol. 25, pp. 209-216, ISSN 0008-0594.
- Miyaji, F.; Kono, Y. & Suyama, Y. (2005). Formation and structure of zinc-substituted calcium hydroxyapatite. *Materials Research Bulletin*, Vol. 40, pp. 209–220, ISSN 0025-5408
- NIST Standard Reference Database 46, version 7 (2003) *NIST Critically Selected Stability Constants of Metal Compounds*, MD 20899 Gaithersburg, USA.
- Oyane, A.; Kim, H.M.; Furuya, T.; Kokubo, T.; Miyazaki, T. & Nakamura, T. (May 2003) Preparation and assessment of revised simulated body fluids. *J. Biomed. Mater. Res.*, Vol. 65A, pp. 188-195, ISSN 1552-4965.
- Palmer, L. C.; Newcomb, C. J.; Kaltz, S. R.; Spoerke, E. D. & Stupp, S. I. (2008). Biomimetic Systems for Hydroxyapatite Mineralization Inspired By Bone and Enamel. *Chem. Rev.*, Vol. 108, No. 11, pp. 4754–4783, PMID 19006400
- Parkhurst, D.L. (1995) User's guide to PHREEQC-A computer program for speciation, reaction-path, advective-transport, and inverse geochemical calculations. U.S. Geological Survey Water-Resources Investigations Report 95-4227 http://wwwbrr.cr.usgs.gov/projects/GWC_coupled/phreeqci/

- Pearson, R. (1963). Hard and soft acids and bases, *J. Am. Chem. Soc.*, Vol. 85, No 22 (November, 1963), pp. 3533–3539, ISSN 0002 - 7863
- Petrov, O.E.; Dyulgerova, E.; Petrov, L. & Popova, R. (2001) Characterization of calcium phosphate phases obtained during the preparation of sintered biphasic Ca-P ceramics. *Materials Letters*, Vol. 48, pp. 162-167, ISSN 0167-577X
- Rabadjieva, D.; Gergulova, R.; Titorenkova, R.; Tepavitcharova, S.; Dyulgerova, E.; Balarew, Chr. & Petrov, O. (2010) Biomimetic transformations of amorphous calcium phosphate: kinetic and thermodynamic studies. *J Mater Sci: Mater Med.*, Vol. 21, No 9, pp. 2501-2509, ISSN 1573-4838
- Radin, S. R. & Ducheyne, P. (1993) Effect of bioactive ceramic composition and structure on in vitro behavior. II. Precipitation. *J Biomed Mater Res*, Vol. 27, pp. 35–44, ISSN 1549-3296.
- Radin, S. R. & Ducheyne, P. (1994) Effect of bioactive ceramic composition and structure on in vitro behavior. III. Porous versus dense ceramics. *J Biomed Mater Res.*, Vol. 28, pp. 1303–1309, ISSN 1549-3296.
- Raghuvir S.; Kurella, A. & Narendra B. D., (2006). Laser Surface Modification of Ti–6Al–4V: Wear and Corrosion Characterization in Simulated Biofluid. *J Biomater App*, Vol. 21, pp. 49 - 73, ISSN 0885-3282
- Shibli, S.M. & Jayalekshmi, A.C. (2009) A novel nano hydroxyapatite-incorporated Ni-P coating as an effective inter layer for biological applications. *J Mater Sci: Mater Med*, Vol. 20, pp. 711–718, ISSN 0957-4530
- Sinyaev, V.A.; Shustikov, E.S.; Levchenko, .LV. & Sedunov, A.A, (2001) Synthesis and dehydration of amorphous calcium phosphate. *Inorganic Materials*, Vol. 37, pp. 619-622, ISSN 0020-1685
- Sykora, V. (1976) *Chemicko analytické tabulky*, DT 543(083), Praha, Czech Republic.
- Tas, A. C. (2004) Participation of Calcium Phosphate Bone Substitutes in the Bone Remodeling Process Influence of Materials Chemistry and Porosity. *Key Engineering Materials*, Vol. 264-268, pp. 1969-1972, ISSN 1662-9795
- Teixeira, C.C.; Nemelivsky, Y.; Karkia, C. & Legeros, R.Z. (2006) Biphasic calcium phosphate: a scaffold for growth plate chondrocyte maturation. *Tissue Eng.*, Vol. 12, No 8 (August, 2006), pp. 2283-9,
- Todorov, T.; Rabadjieva, D. & Tepavitcharova, S. (2006). New thermodynamic database for more precise simulation of metal species in natural waters. *Journal of the University of Chemical Technology and Metallurgy*. Vol. 41, pp. 97-102. ISSN 1311-7629
- Tung, M.S.; Eidelman, N.; Sieck, B. & Brown, W.E. (1988) Octacalcium phosphate solubility product from 4 to 37°C. *J Res Natl Bur Stand*, Vol. 93, pp. 613-624, ISSN 0022-4332
- Xiaobo, Ch.; Yuncang, L.; Peter, D.H. & Cui'e, W. (2009) Microstructures and bond strengths of the calcium phosphate coatings formed on titanium from different simulated body fluids. *Materials Science and Engineering*, Vol. C 29, pp. 165-171, ISSN 0928-4931

Xue, W.; Dahlquist, K.; Banerjee, A.; Bandyopadhyay, A. & Bose, S. (2008) Synthesis and characterization of tricalcium phosphate with Zn and Mg based dopants. *J Mater Sci: Mater Med*, Vol.19, pp. 2669-2677, ISSN 0957-4530.

IntechOpen

IntechOpen



On Biomimetics

Edited by Dr. Lilyana Pramatarova

ISBN 978-953-307-271-5

Hard cover, 642 pages

Publisher InTech

Published online 29, August, 2011

Published in print edition August, 2011

Bio-mimicry is fundamental idea – How to mimic the Nature™ by various methodologies as well as new ideas or suggestions on the creation of novel materials and functions. This book comprises seven sections on various perspectives of bio-mimicry in our life; Section 1 gives an overview of modeling of biomimetic materials; Section 2 presents a processing and design of biomaterials; Section 3 presents various aspects of design and application of biomimetic polymers and composites are discussed; Section 4 presents a general characterization of biomaterials; Section 5 proposes new examples for biomimetic systems; Section 6 summarizes chapters, concerning cells behavior through mimicry; Section 7 presents various applications of biomimetic materials are presented. Aimed at physicists, chemists and biologists interested in biomineralization, biochemistry, kinetics, solution chemistry. This book is also relevant to engineers and doctors interested in research and construction of biomimetic systems.

How to reference

In order to correctly reference this scholarly work, feel free to copy and paste the following:

Diana Rabadjieva, Stefka Tepavitcharova, Kostadinka Sezanova, Romyana Gergulova, Rositsa Titorenkova, Ognyan Petrov and Elena Dyulgerova (2011). Biomimetic Modifications of Calcium Orthophosphates, *On Biomimetics*, Dr. Lilyana Pramatarova (Ed.), ISBN: 978-953-307-271-5, InTech, Available from: <http://www.intechopen.com/books/on-biomimetics/biomimetic-modifications-of-calcium-orthophosphates>

INTECH
open science | open minds

InTech Europe

University Campus STeP Ri
Slavka Krautzeka 83/A
51000 Rijeka, Croatia
Phone: +385 (51) 770 447
Fax: +385 (51) 686 166
www.intechopen.com

InTech China

Unit 405, Office Block, Hotel Equatorial Shanghai
No.65, Yan An Road (West), Shanghai, 200040, China
中国上海市延安西路65号上海国际贵都大饭店办公楼405单元
Phone: +86-21-62489820
Fax: +86-21-62489821

© 2011 The Author(s). Licensee IntechOpen. This chapter is distributed under the terms of the [Creative Commons Attribution-NonCommercial-ShareAlike-3.0 License](#), which permits use, distribution and reproduction for non-commercial purposes, provided the original is properly cited and derivative works building on this content are distributed under the same license.

IntechOpen

IntechOpen